Autophagy

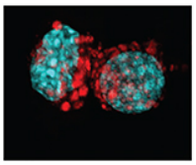

Autophagy

ISSN: 1554-8627 (Print) 1554-8635 (Online) Journal homepage: www.tandfonline.com/journals/kaup20

Duloxetine ameliorates cerebral ischemic injury by inhibiting autophagy

Alice Viotti , Claudia Molinaro , Jessica Perego , Andrea Fossaghi , Chiara Parravicini , Eliana Lauranzano , Antonella Borreca , Marco Piccoli , Luigi Anastasia , Susanna Manenti , Annamaria Finardi , Alessandra Mandelli , Michela Matteoli , Ivano Eberini , Paola Panina , Gianvito Martino & Luca Muzio

To cite this article: Alice Viotti , Claudia Molinaro , Jessica Perego , Andrea Fossaghi , Chiara Parravicini , Eliana Lauranzano , Antonella Borreca , Marco Piccoli , Luigi Anastasia , Susanna Manenti , Annamaria Finardi , Alessandra Mandelli , Michela Matteoli , Ivano Eberini , Paola Panina , Gianvito Martino & Luca Muzio (2026) Duloxetine ameliorates cerebral ischemic injury by inhibiting autophagy, Autophagy, 22:6, 1306-1332, DOI: 10.1080/15548627.2026.2641616

To link to this article: https://doi.org/10.1080/15548627.2026.2641616

AUTOPHAGY
2026, VOL. 22, NO. 6, 1306–1332
https://doi.org/10.1080/15548627.2026.2641616

Taylor & Francis
Taylor & Francis Group

RESEARCH PAPER

Duloxetine ameliorates cerebral ischemic injury by inhibiting autophagy

Alice Viotti[a], Claudia Molinaro[a], Jessica Perego[a], Andrea Fossaghi[a], Chiara Parravicini[b], Eliana Lauranzano[c], Antonella Borreca[c,d], Marco Piccoli[e], Luigi Anastasia[e], Susanna Manenti[f], Annamaria Finardi[f], Alessandra Mandelli[f], Michela Matteoli[d,g], Ivano Eberini[b], Paola Panina[a,h], Gianvito Martino[a], and Luca Muzio [a*]

[a]Neuroimmunology Unit, Institute of Experimental Neurology (INSPE), Division of Neuroscience, IRCCS San Raffaele Scientific Institute, Milan, Italy; [b]Dipartimento di Scienze Farmacologiche e Biomolecolari "Rodolfo Paoletti", Università degli Studi di, Milano, Italy; [c]Pharmacology and Brain Pathology Unit, IRCCS Humanitas Research Hospital, Rozzano, Milan, Italy; [d]Consiglio Nazionale delle Ricerche, URT c/o IRCCS Humanitas Research Hospital, Neuroscience Institute, Milan, Italy; [e]Stem Cells for Tissue Engineering Lab, IRCCS Policlinico, San Donato, San Donato M.se, Italy; [f]Clinical Neuroimmunology Unit, Institute of Experimental Neurology (INSPE), Division of Neuroscience, IRCCS San Raffaele Scientific Institute, Milan, Italy; [g]Department of Biomedical Sciences, Humanitas University, Pieve Emanuele, Milan, Italy; [h]Department of Neuroscience, Università Vita e Salute San Raffaele, Milan, Italy

ABSTRACT

Ischemic stroke is a severe medical condition characterized by diminished blood flow to the brain, resulting in a shortage of oxygen and nutrients. During ischemia, neurons surrounding the cerebral infarct initiate macroautophagy. However, the implications of this activation for neuronal cell survival are still debated. The identification of new autophagy modulators could aid in understanding autophagy's role in brain ischemia and lay the groundwork for innovative therapeutic strategies aimed at minimizing brain damage in this life-threatening neurological emergency. In this study, we developed a robust and sensitive screening platform to identify autophagy modulators from a library of bioactive compounds. Selected compounds underwent further *in vitro* validation, leading to the identification of duloxetine, a Food and Drug Administration (FDA)-approved drug, as an effective autophagy inhibitor at low-micromolar concentrations. Following its original characterization, the molecule, a serotonin-norepinephrine re-uptake inhibitor (SNRI) family member, was subsequently tested in young and aged mice subjected to photothrombotic stroke. Our results demonstrated that duloxetine significantly reduced infarct size and improved locomotor performance in mice that had undergone a stroke. Similar protective effects were observed in transgenic mice lacking the autophagy gene *Atg5* (autophagy related 5) in SLC17A6/Vglut2$^+$ (solute carrier family 17 member 6) excitatory cortical neurons. Finally, we elucidated the underlying mechanism of action that involves duloxetine-mediated inhibition of TRPM2 (transient receptor potential cation channel subfamily M member 2) ion channels. Altogether, our findings suggest that early autophagy inhibition is neuroprotective in stroke, and duloxetine serves as an effective means of achieving this inhibition.

ARTICLE HISTORY
Received 26 June 2025
Revised 29 January 2026
Accepted 3 March 2026

KEYWORDS
Brain ischemia; duloxetine; macroautophagy; SNRI; TRPM2

Abbreviation: AMPK - AMP-activated protein kinase; ATG5 - autophagy related 5; AVs - autophagic vacuoles; Baf -bafilomycin A_1; BBB - blood-brain barrier; BECN1 -beclin 1; CAMK2 -calcium/calmodulin dependent protein kinase II; cCASP3 -cleaved CASP3; cKO -conditional knockout; CNS -central nervous system; DMPK - drug metabolism and pharmacokinetics; DMSO -dimethyl sulfoxide; DIV - days *in vitro*; DMEM - Dulbecco's modified Eagle's medium; FDA - Food and Drug Administration; FBS -fetal bovine serum; GFP -green fluorescent protein; GFAP -glial fibrillary acidic protein; HIF1A/HIF-1α - hypoxia inducible factor 1 subunit alpha; HMGCR - 3-hydroxy-3-methylglutaryl-CoA reductase; IHC - immunohistochemistry; I/R – ischemia-reperfusion; LAMP1 - lysosomal associated membrane protein 1; MAP1LC3B/LC3B -microtubule associated protein 1 light chain 3 beta; MCAO - middle cerebral artery occlusion; MFI -mean fluorescence intensity; MTT - 3-[4,5-dimethylthiazol-2-yl]-2,5 diphenyl tetrazolium bromide; ND -nutrient deprivation; NPCs -neural precursor cells; NVU -neuro-vascular unit; OGD - oxygen-glucose deprivation; PI - propidium iodide; PIKK - phosphatidylinositol 3-kinase-like; PRKDC/DNA-PKcs - protein kinase, DNA-activated, catalytic subunit; SQSTM1/p62 -sequestosome 1; PIK3C3/VPS34 - phosphatidylinositol 3-kinase catalytic subunit type 3; PK-hLC3 -pHluorin-mKate2-human LC3; PLP1 - proteolipid protein 1; PT - photothrombotic; ROS -reactive oxygen species; SLC17A6/Vglut2 - solute carrier family 17 member 6; S:*N* –signal-to-noise; SSMD - strictly standardized mean difference; SNRIs - serotonin and norepinephrine reuptake Inhibitors; TTC - 2,3,5-triphenyltetrazolium chloride; TEER - transendothelial electrical resistance; TEM - transmission electron microscopy; TRPM2 -transient receptor potential cation channel subfamily M member 2; TBI -traumatic brain injury; ULK1 - unc-51 like autophagy activating ainase 1; V-ATPase - vacuolar-type H^+-translocating ATPase.

CONTACT Luca Muzio muzio.luca@hsr.it Neuroimmunology Unit, Institute of Experimental Neurology (INSPE), Division of Neuroscience, IRCCS Ospedale San Raffaele, Milan 20132, Italy

*These authors jointly supervised this work.

Supplemental data for this article can be accessed online at https://doi.org/10.1080/15548627.2026.2641616

Introduction

Ischemic stroke, a leading cause of morbidity and mortality worldwide, occurs when a blood clot obstructs a cerebral artery [1]. The abrupt decrease in cerebral blood flow causes ischemia and the initiation of a series of molecular events that trigger tissue damage, leading to the death of neuronal, glial, and endothelial cells, and culminating in neurological deficits. Despite some advances in acute stroke management, current therapeutic options, including thrombolysis and mechanical thrombectomy, have several limitations, and the post-stroke therapeutic window remains narrow [2]. Consequently, there is an urgent need for novel therapeutic strategies that can mitigate damage and promote recovery in the post-stroke period.

Macroautophagy (herein referred to as autophagy) is a highly conserved cellular degradation and recycling process, essential for maintaining cellular homeostasis and supplying nutrients to sustain cellular metabolism during various forms of stress. In the context of the ischemic stroke, autophagy is rapidly activated as a response to energy depletion and cellular stress, including excitotoxicity, oxidative stress, and inflammation [3]. The shortage of oxygen and glucose leads to ATP depletion, causing an energy crisis in cells culminating in the accumulation of damaged organelles and proteins. The upregulation of autophagy is thought to serve as a compensatory mechanism, recycling these damaged components to sustain cellular metabolism. Key autophagy regulators during ischemic stroke include the AMPK (AMP-activated protein kinase)-MTOR (mechanistic target of rapamycin kinase) signaling pathway and HIF1 (hypoxia inducible factor 1) [4–7]. Autophagy activation is marked by increases in MAP1LC3/LC3 (microtubule associated protein 1 light chain 3) and BECN1 (beclin 1) levels in brain neurons of stroke models [8]. Similarly, autophagosome formation is elevated in neurons of neonatal ischemic brains, and such upregulation has been associated with hippocampal neuronal death [9]. Although the activation of the autophagic cascade in neurons, astrocytes, and endothelial cells is commonly observed in brain ischemia models [10–13], it remains debated whether such activation is entirely protective. Thus, a dual-faceted role for autophagy activation in brain ischemia has emerged in recent scientific literature.

The induction of autophagy promotes cell survival by removing damaged organelles and providing essential substrates for energy production. A balanced activation of autophagy appears to be beneficial in ischemic conditions, as it limits neuronal apoptosis and promotes cell survival. Supporting this view, the autophagy inducer rapamycin has proven effective in experimental models of stroke [14]. Similarly, the modulation of the of the neuron-specific conventional PRKCG/cPKCγ (protein kinase C gamma-AKT)-MTOR cascade improved neuronal outcomes in mice subjected to cerebral ischemia [15].

However, accumulating evidence also indicates that excessive or prolonged autophagy can contribute to neuronal injury and cell death, thereby exacerbating ischemic damage [16]. Consistent with this, studies using the permanent middle cerebral artery occlusion (pMCAO) model have shown that pharmacological inhibition of autophagy markedly reduces ischemic volume, brain edema, and motor deficits in rats [17].

Understanding the fine balance between beneficial and harmful autophagy is therefore essential for developing targeted therapeutic strategies in stroke that may open promising therapeutic avenues. Although prolonged autophagy activation in the early post-stroke phases may exert detrimental effects, a balanced modulation of autophagy could result in neuroprotection without causing excessive autophagy-mediated cell death. Compounds like trehalose and spermidine, which mildly activate autophagy, have shown neuroprotective effects [18,19]. Current research on neuroprotective therapeutics has identified additional candidates that indirectly modulate autophagy. Among them, Statins, which inhibit the HMGCR (3-hydroxy-3-methylglutaryl-CoA reductase) involved in cholesterol metabolism, affect autophagy in stroke models. Indeed, amlodipine and atorvastatin reducing LC3-positive cells also reduced the infarct volume in a stroke model [20]. Simvastatin has also shown neuroprotective effects after spinal cord injury, partially through the AKT-MTORC1 signaling pathway [21]. Traditional Chinese drugs have proven beneficial through autophagy regulation. For instance, puerarin alleviated brain injury after ischemia-reperfusion damage by selectively reducing the expression of autophagic proteins in neurons [22]. Likewise, triptolide reduces the infarct size by modulating autophagy and apoptosis pathways occurring post-MCAO induction [23].

We aim to identify chemical modulators that selectively target the autophagic pathway under ischemic-like conditions. To this end, we developed a robust low-throughput screening platform to test a library of bioactive compounds under stroke-mimicking conditions, followed by *in vitro* validation of lead compounds and *in vivo* validation using a mouse model of photothrombosis (PT).

Results

In silico *pharmacokinetic analysis to improve drug screening of CNS-active compounds*

We screened a commercially available library of drug-like small molecules (Selleckchem Bioactive Compound Library-I) for autophagy modulators, using a primary fluorescence-based assay followed by *in vitro* and *in vivo* validation (Figure 1A). Drug metabolism and pharmacokinetics (DMPK) properties of these molecules were predicted *in silico* using a set of molecular descriptors (Table 1) and compared to well-characterized bioactive molecules. From the original dataset of 6839 compounds, 45 were discarded due to missing structural information or processing issues during computational analyses. Among all the selection criteria provided by the prediction tool, we prioritized those related to drug-likeness and central nervous system (CNS) penetration and activity. Drug-likeness was evaluated by computing QPlogPo/w, #stars, RuleOfFive, RuleOfThree, #metab, and #rtvFG parameters (Fig. S1A-F). We implemented the analysis using additional molecular

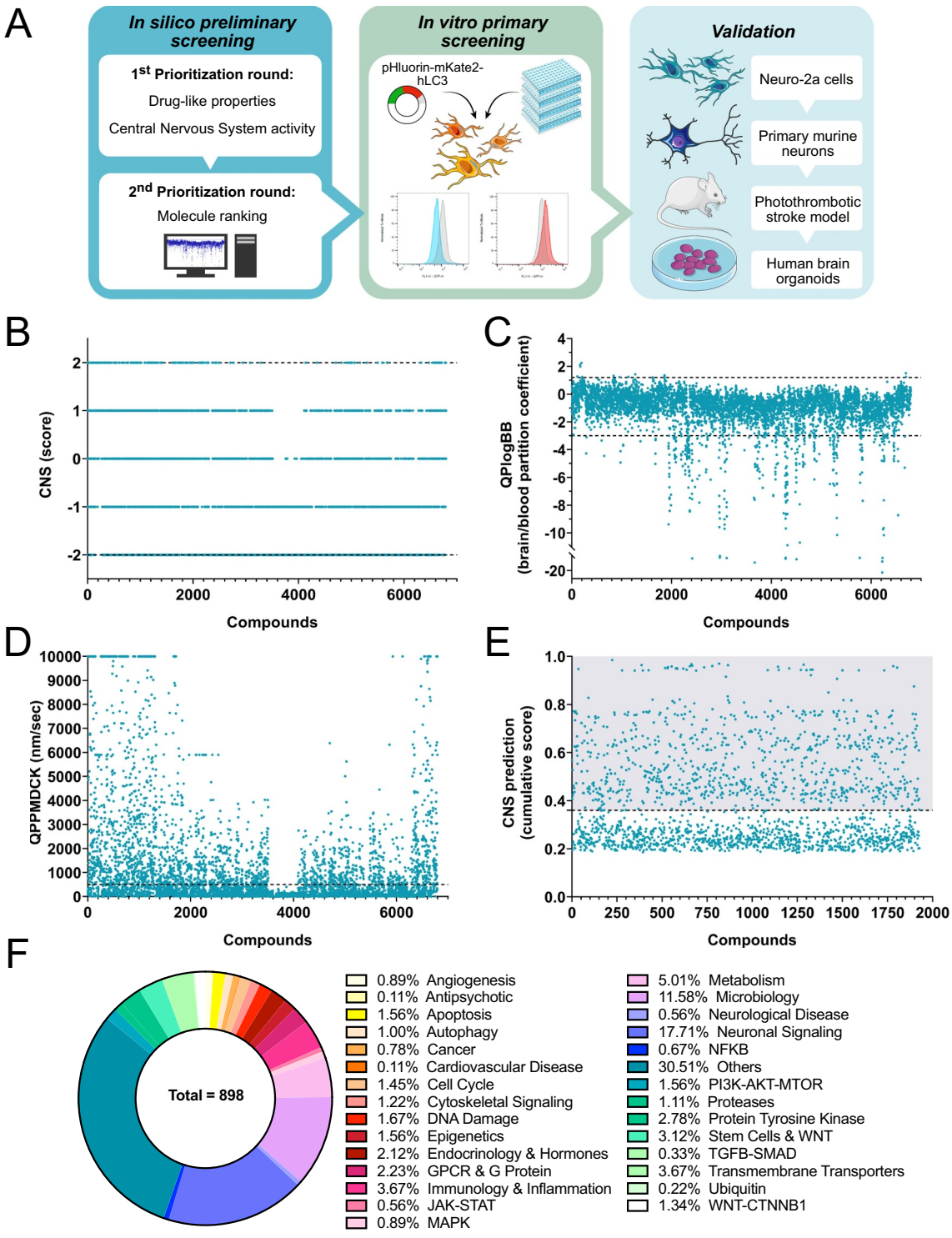

Figure 1. Study overview and *in silico* compounds selection based on drug-like and CNS-related properties. (A) Graphical representation of the study workflow. (B-D) Graphs showing the dispersion of compounds based on CNS (B), QPlogBB (C), and QPPMDCK (D) score prediction. Ranges for 95% of known drugs are highlighted by dashed lines. (E) CNS activity and penetration properties (cumulative score) of the selected 1927 compounds. The shaded area encloses selected compounds with a score higher than 0.367. Each dot represents a single molecule. (F) Graphical representation of the composition of selected compound library based on known target pathways.

descriptors that are predictive of CNS activity: CNS, QPlogBB, QPPMDCK (Figure 1B-D). After the initial prioritization, we identified 1927 compounds (28.17% of the original dataset) with computed properties within the acceptable range of known drugs. Molecules excluded from the analyses (71.83%) had at least one computed descriptor that was outside the normal range of known drugs. A subsequent round of *in silico* prioritization was conducted to obtain desirable features for CNS-active drugs. We assigned a cumulative score to each compound by linearly integrating CNS, QPlogBB, and QPPMDCK descriptors. Compounds with a cumulative score exceeding a threshold of 0.367 were selected for further analysis. This approach resulted in the selection of 898 bioactive compounds (13.13% of the library, Figure 1E). The selected

Table 1. *In silico* DMPK parameters used in the present study.

Property or Descriptor	Range (for 95% of known drugs)	Description
QPlogPo/w	−2.0 to 6.5	Predicted octanol/water partition coefficient
#stars	0 to 5	Number of property or descriptor values that fall outside the 95% range for known drugs
RuleOfFive	Maximum is 4	Number of violations of Lipinski's rule of five
RuleOfThree	Maximum is 3	Number of violations of Jorgensen's rule of three
#metab	1 to 8	Number of likely metabolic reactions
#rtvFG	0 to 2	Number of reactive functional groups
CNS	−2 to +2	Predicted CNS activity
QPPMDCK	<25 poor; >500 great	Predicted apparent MDCK cells permeability in nm/sec
QPlogBB	−3.0 to 1.2	Predicted brain/blood partition coefficient

The table shows the *in silico* parameters used to predict the pharmacokinetic and pharmacodynamic properties of drug candidates. The listed descriptors, along with their corresponding ranges for 95% of known drugs, have been utilized to assess critical characteristics such as drug permeability, central nervous system activity, and metabolic behavior.

library was quite heterogeneous as the compounds fell into 19 different biological categories (Figure 1F). Of note, over 350 molecules in the final list are currently Food and Drug Administration (FDA)-approved drugs.

Chemical screening identified novel autophagy modulators

The primary screening assay, designed to monitor the autophagic flux in Neuro-2a cells, took advantage of the tandem fluorescent protein-tagged LC3 reporter, pHluorin-mKate2-human LC3 (PK-hLC3) [24]. This LC3 chimera comprises the human LC3 protein and pHluorin, a pH-sensitive green fluorescent protein (GFP) variant whose fluorescence is rapidly quenched when the protein is exposed to an acidic environment [24]. Transfected Neuro-2a cells were selected by puromycin, followed by limiting dilution to obtain single cell-derived clones. By confocal microscopy we scored PK-hLC3 fluorescence levels in cells treated with either the inhibitor of the vacuolar-type H^+-translocating ATPase (V-ATPase) bafilomycin A_1 (Baf) [25] or with the MTOR inhibitor torin-1 [26,27]. We selected the 7B11 cell clone, which showed increased pHluorin fluorescence intensity levels after Baf treatment and decreased fluorescence levels in response to torin-1 (Figure 2A).

Western blot analysis of parental Neuro-2a cells, Neuro-2a cells transiently transfected with PK-hLC3 plasmids, and 7B11 cells treated with autophagy modulators showed that Baf treatment increased the accumulation of endogenous LC3-II in all three groups (Fig. S2A and B). Torin-1 increased LC3-II levels in both parental and 7B11 cells; however, such modulation was evident only as a trend in cells expressing the PK-hLC3 plasmid (Fig. S2B), thus suggesting that the overexpression of plasmids encoding PK-hLC3 in Neuro-2a cells may impact on the conversion of the endogenous LC3-I to LC3-II. The co-stimulation of cells with Baf and torin-1 enhanced LC3-II levels in parental Neuro-2a cells and 7B11 cells, albeit such upregulation in 7B11 cells was only a trend when compared to Baf alone (Fig. S2A and B). A ~ 65 kDa band corresponding to the PK-hLC3 fusion protein was detected in 7B11 cells, although we were unable to detect a clear molecular weight shift deriving from addition of phosphatidylethanolamine (PE) (Fig. S2A and B).

We used flow cytometry in 7B11 cells to assess variations of the autophagic flux in response to torin-1 and Baf (Figure 2B) [28]. Mean fluorescence intensity (MFI) levels of pHluorin increased in response to Baf, while decreased following torin-1 exposure (Figure 2B and S2C for signal acquisition strategies). To assess performance and reproducibility of the assay we measured pHluorin MFI levels in response to Baf and torin-1 across six consecutive experiments using cells from the same batch (Fig. S2D and E). PHluorin MFI levels were used to calculate the Z'-factor and the strictly standardized mean difference (SSMD) [29]. By applying a Z'-factor in the range of 0.5 to 1 and an SSMD cutoff β values of ≥4.7 for Baf and ≤−4.7 for torin-1, we observed statistically significant differences between treatments and controls in at least four consecutive experimental runs (Fig. S2F and G; Table 2).

Oxygen-glucose deprivation (OGD) is an ischemic stressor that activates the autophagic flux in neurons [30,31]. OGD decreased PK-hLC3 MFI levels in 7B11 cells, and such reduction linearly correlated with the length of the treatment (Figure 2B,C) [32]. Since an excessive activation of the autophagic flux can affect cell survival, inducing a self-digestion process [8], we limited the OGD treatment to 15 h – sufficient to reduce pHluorin MFI by 25% while preserving cell viability (Figure 2D and S2H). As expected, the OGD treatment substantially increased HIF1A/HIF-1α levels (Fig. S2I) [33].

Each compound was incubated on OGD-treated 7B11 cells at the concentration of 1 μM for 15 h. Cells were then allowed to reoxygenate for 2 h to replicate the ischemia-reperfusion (I/R) model (Figure 2E). Internal quality controls were included in each plate, incubating 7B11 cells with Baf and/or torin-1 (Figure 2F). To identify hits that modulate the autophagic flux in the I/R paradigm, average MFI levels from compound-treated cells were compared to OGD-reoxygenation controls. Signal-to-noise (S:N) ratio calculated in each experimental run and comparing untreated and OGD-treated 7B11 cells was used to assess the general quality of the assay. Only plates displaying a S:N higher than 2 were included in the analysis (Figure 2H).

Among the 22 selected hits, 7 molecules activated the autophagic flux under I/R conditions, while 15 inhibited it (Figure 2G and Table S1). Of the 898 tested compounds, 97% did not significantly modulate pHluorin MFI levels. Seventeen molecules exhibited moderate to high toxicity and were excluded from the analysis. Three compounds, namely ULK-

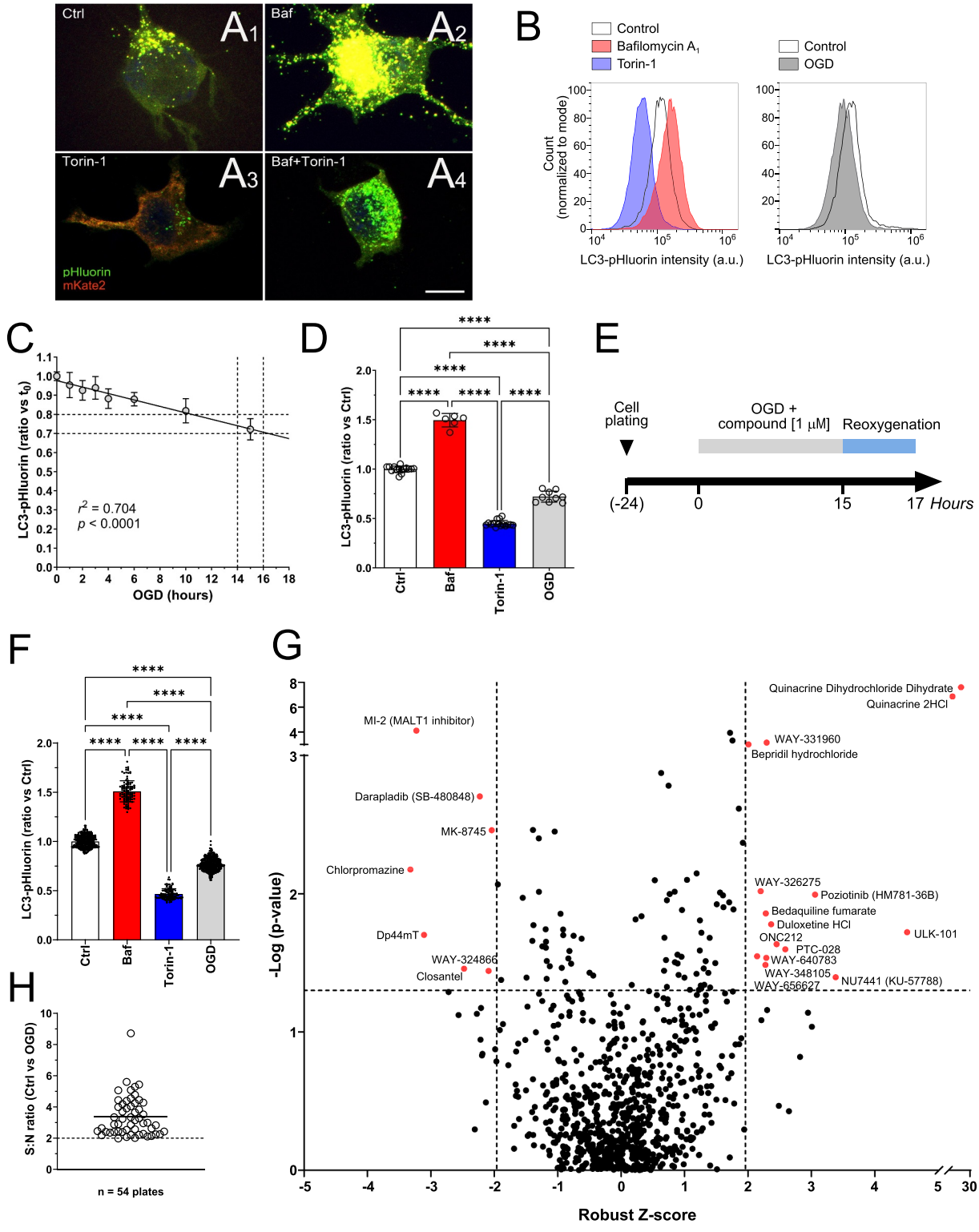

Figure 2. Identification of autophagy modulators in 7B11 cells using fluorescent-based drug screening. (A_{1-4}) Maximal projections confocal images of 7B11 cells showing PK-hLC3 and mKate2 distributions ($n = 3$ covers/condition) in control (A_1) (Ctrl); (A_2) Baf (200 nM, 6 h); (A_3) torin-1 (250 nM, 24 h) and (A_4) Baf+torin-1 cells. (B) Representative histograms showing pHluorin fluorescence intensity (x-axis) versus mode-normalized event count (y-axis) obtained by flow cytometry ($n \geq 6$ independent samples/condition). (C) Time course analysis of pHluorin fluorescence intensity during OGD in cells sampled at 0, 1, 2, 3, 4, 6, 10, and 15 h. Data are normalized to time 0 (t_0) and presented as mean ± SD ($n = 9$ independent samples/condition). Vertical dashed lines indicate the time window for a 25% fluorescence decrease ($r^2 = 0.704$, $p < 0.0001$). (D) Histogram shows quantifications of pHluorin fluorescence in 7B11 cells treated with: DMSO (Ctrl), Baf (200 nM, 15 h), torin-1 (250 nM, 24 h) and OGD (15 h). Values (mean ± SD) are normalized to DMSO-treated control; dots show independent wells. (E) Timeline of the experimental procedure. (F) Comprehensive quantification of pHluorin fluorescence intensity from the following experimental controls (mean ratio vs Ctrl ± SD): ctrl ($n = 347$ wells), Baf ($n = 111$ wells, 200 nM, 15 h), torin-1 ($n = 111$ wells, 250 nM, 24 h), and OGD ($n = 381$ wells, 15 h). (G) Volcano plot summarizing screening results, showing the robust Z-score (x-axis) and -Log(p-value) (y-axis) from 3 independent replicates; red dots represent 22 lead-like candidates; dashed lines indicate statistical thresholds (see the Table 3 for thresholds). (H) Signal-to-noise ratio (S:N) calculated in each multi-wells plate ($n = 54$). One-way ANOVA followed by Tukey's multiple comparison test was used to analyze data from (D) and (F); significance levels: *$p < 0.05$, **$p < 0.01$, **$p < 0.001$, ****$p < 0.0001$. Scale bar: 10 μm.

Table 2. Z′-factor and SSMD thresholds for data analysis.

Statistical parameter	Assay quality	Range
Z′-factor	Very good	$0.5 \le Z' < 1$
	Acceptable	$0 \le Z' < 0.5$
	Unacceptable	$Z' < 0$
Strictly Standardized Mean Difference	Excellent	$\beta \ge 4.7$; $\beta \le -4.7$
	Good	$3 > \beta \ge 4.7$; $-4.7 < \beta \le -3$
	Inferior	$2 > \beta \ge 3$; $-3 < \beta \le -2$
	Poor	$\beta \ge 2$; $\beta \le -2$

The table outlines the quality of assay performance based on the Z′-factor and SSMD values. The Z′-factor is used to evaluate assay robustness, with a range from very good to unacceptable. SSMD values assess the assay's discriminatory power, with thresholds indicating excellent to poor performance. Z′-factor and SSMD values within the specified ranges indicate the respective quality of the assay.

Table 3. Robust Z-score thresholds for data analysis.

Robust Z-score	p-value	Confidence level
<−1.65 or >1.65	<0.1	90%
<−1.96 or >1.96	<0.05	95%
<−2.58 or >2.58	<0.01	99%

The table outlines the Z-score thresholds used to evaluate statistical significance based on different p-value cutoffs and corresponding confidence levels. The thresholds indicate the range of Z-scores that correspond to p-values below 0.1, 0.05, and 0.01, with confidence levels of 90%, 95%, and 99%, respectively. These thresholds help assess the reliability and statistical significance of the data in the context of hypothesis testing.

101, quinacrine 2HCl, and quinacrine dihydrochloride dihydrate, are known inhibitors of autophagic machinery and were therefore excluded from further validation steps. Specifically, ULK-101 directly inhibits ULK1 (unc-51 like autophagy activating kinase 1), with an IC50 of 8.3 nM [34], and quinacrine operates as an autophagy inhibitor in glioma cells [35].

Experimental validation of pre-screened chemical candidates

We next determined the capacity of selected compounds to modulate LC3-I to LC3-II conversion in naïve Neuro-2a cells [36]. Controls were obtained incubating cells with Baf and/or with torin-1 (Fig. S3A) [36,37]. Compounds were used at the final concentration of 1 μM, along with Baf but in absence of OGD treatment (Figure 3A,B) [38]. On the one hand, similarly to Baf, molecules that inhibit the autophagic flux at later stages should increase LC3-II levels. On the other hand, compounds that exert an early autophagy inhibition should reduce LC3-II conversion – even in the presence of Baf – as shown with the class III phosphatidylinositol 3-kinase (PtdIns3K)-dependent early autophagy inhibitor 3-methyladenine (3-MA) (Fig. S3B) [39].

Unfortunately, WAY-324886 was unavailable from any commercial repositories we inquired and was therefore not tested. Co-incubation of NU7441, poziotinib, ONC212, bedaquiline, duloxetine, or WAY640783 with Baf resulted in a significant reduction of LC3-I to LC3-II conversion, when compared to cells only treated with Baf (Figure 3A, C). In the absence of Baf, MK-8745 and Dp44mT increased LC3-I to LC3-II conversion compared to vehicle-treated cells (Figure 3B,D). Interestingly, we noticed a significant reduction of LC3-II in cells treated with duloxetine alone. Detailed analyses of the compounds involved in this validation are reported in Figure S3C-H and Figure S4A-F.

Hits were further validated by dose-response experiments in Neuro-2a cells (ranging from 0.1 μM to 10 μM). Compounds that were hypothesized to inhibit autophagic flux were still tested in the presence of Baf, while Baf was omitted for compounds we believed to act as activator of autophagy. Under Baf treatment, NU7441, duloxetine, ONC212, and poziotinib decreased LC3-II levels according to dose-response relationship (Figure 3E-L). Bedaquiline and WAY-640783 failed to modulate LC3-II levels in a dose-dependent manner and were therefore discarded (Fig. S5A and B). Molecules expected to act as inducers of the autophagic flux did not show a linear correlation between LC3-II levels and their concentrations (Fig. S5C and D).

We scored autophagic vesicles (AVs) by transmission electron microscopy (TEM) on naive Neuro-2a cells [40]. We established the baseline using vehicle-treated controls. Blocking protein degradation after autophagosomes-lysosomes fusion with Baf increased both the number and the size of AVs (Figure 4A,B,L,K). Torin-1 increased the number but not the size of AVs, suggesting that it enhanced AVs formation but also promoted rapid degradation of their content (Figure 4A,C,K,L). Blocking protein degradation with Baf and reducing the generation of new AVs with 3-MA [39,41,42] increased the number of AVs but not their size (Figure 4D,K,L).

Cells treated with NU7441 and Baf showed a substantial reduction of both the number and the size of AVs (Figure 4E, K,L). AVs numbers in cells treated with duloxetine, ONC212, and poziotinib alongside Baf increased when compared with vehicle-treated controls, mirroring results obtained in cells treated with both Baf and 3-MA (Figure 4F,G,H,K,L). However, these 3 compounds caused the swelling of AVs in cells, suggesting that AVs accumulated undigested material. MK-8745 and Dp44mT, which were hypothesized to be autophagy activators, were tested without Baf. Both molecules behaved similarly to torin-1, confirming their pro-autophagic activity at this working concentration (Figure 4C, I-L).

We next established an *in vitro* model of neuro-vascular unit (NVU) [43]. Primary brain endothelial cells were left to mature on the apical side of a matrix-coated transwell insert, in direct contact with primary glial cells on the basolateral side. 7B11 cells were co-cultured downstream of the NVU model and stimulated or not with Baf in the basolateral compartment. The transwell containing the NVU prototype was then added to the wells with the cells (Fig. S5E). Characterization of the physiological properties of the blood-brain barrier (BBB) model – in terms of transendothelial electrical resistance (TEER) and the paracellular diffusion of water-soluble substances/Pe – were evaluated in response to selected compounds. A clear effect of Baf on the NVU model was observed, both in terms of reduced resistance (Fig. S5F) and increased dextran permeability (Fig. S5G). Most compounds behaved like dimethyl sulfoxide (DMSO) control, except for duloxetine, which

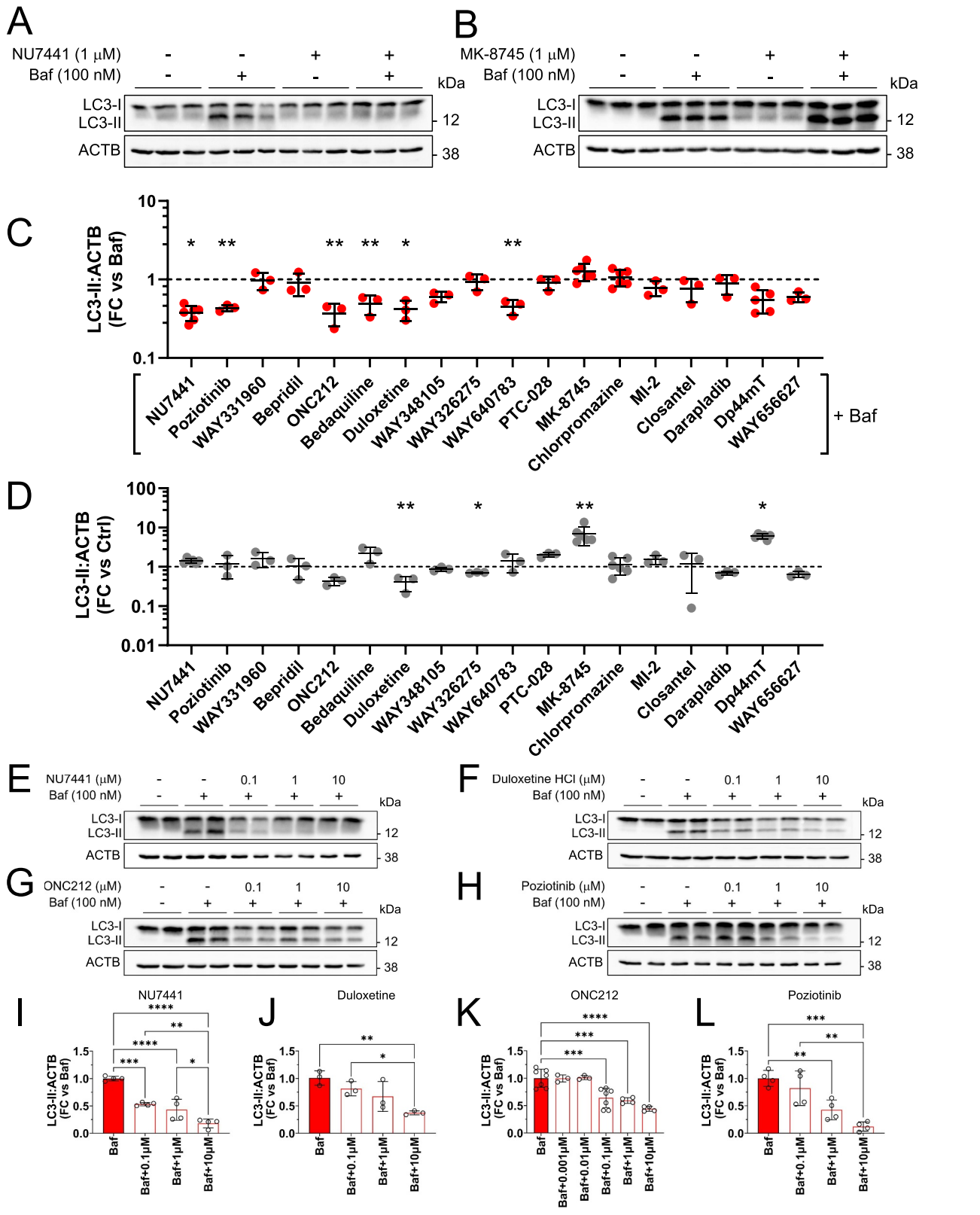

Figure 3. Validation of selected lead-like compounds in parental Neuro-2a cells. (A and B) western blot for MAP1LC3/LC3 and ACTB/β-actin in Neuro-2a cells treated with DMSO (Ctrl), 100 nM Baf with or without 1 μM NU7441 (A), or 1 μM MK-8745 (B), for 15 h. (C and D) Validation of 18 compounds reported as ACTB/β-actin-normalized LC3-II Fold changes; (C) columns show 1 μM single compounds + Baf Fold changes relative to Baf alone; (D) columns show 1 μM single compounds Fold changes relative to DMSO alone (Ctrl). (E-H) western blot for MAP1LC3/LC3 and ACTB/β-actin in Neuro-2a cells treated with 100 nM baf as well as with Baf + increasing concentrations of each compound (0.1, 1, 10 μM) for 15 h; quantifications are shown in histograms (I-L) (mean ratio vs Baf ± SD; $n \geq 3$ independent wells). Unpaired Student's t-test was used to analyze data from (C) and (D), and one-way ANOVA followed by Tukey's multiple comparison test was used to analyze data from (I-L); significance levels: *$p < 0.05$, **$p < 0.01$, ***$p < 0.001$, ****$p < 0.0001$.

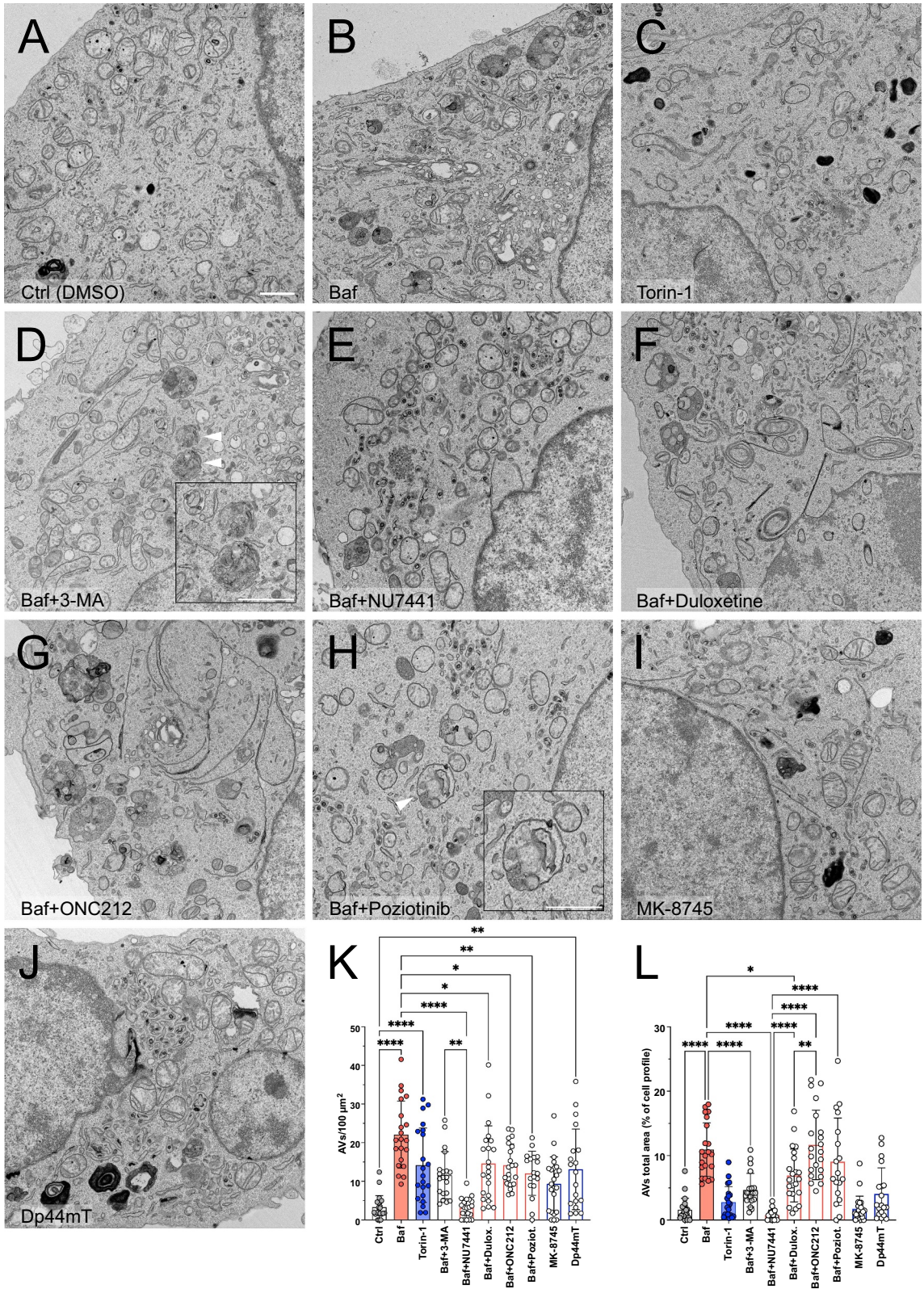

Figure 4. TEM analysis of autophagic vacuoles. (A-J) EM micrographs of Neuro-2a cells treated for 15 h with DMSO (Ctrl) (A), 100 nM Baf (B), 250 nM torin-1 (C), Baf with 5 mM 3-methyladenine (3-MA) (D), Baf and NU7441, duloxetine, ONC212, or poziotinib (10 µM) (E-H); MK-8745 or Dp44mT (10 µM) (I and J). (D and H) Insets: high-magnification images of autophagic vacuoles (AVs). (K) Quantification of the total number of AVs normalized to 100 µm^2, reported as mean ± SD based on $n \geq 18$ micrographs per condition. (L) Total area occupied by AVs in individual cells, presented as mean ± SD from $n \geq 18$ micrographs per condition. Individual cells are represented by dots in the histograms. One-way ANOVA followed by Tukey's multiple comparison test was used to analyze both datasets; significance levels: *$p < 0.05$, **$p < 0.01$, ***$p < 0.001$, ****$p < 0.0001$. Scale bar: 1 µm.

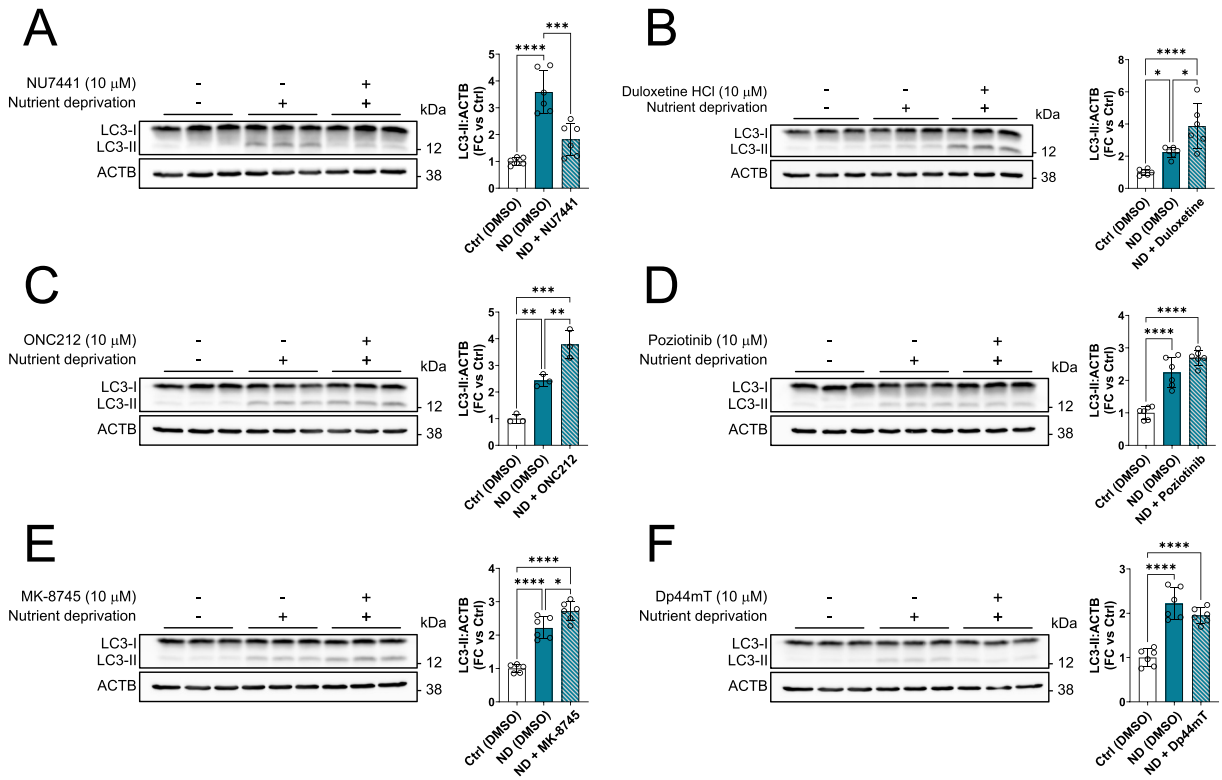

Figure 5. Neuronal validation of lead-like compounds. (A-F) Western blot analysis of MAP1LC3/LC3 and ACTB/β-actin in total protein extracts from neuronal cultures treated for 15 h with nutrient deprivation (ND) with or without selected compounds (10 μM) ($n \geq 3$ independent wells). Histograms on the right of each picture (A-F) show quantifications (mean ratio vs Ctrl ± SD). One-way ANOVA followed by Tukey's multiple comparison test was used to analyze data; significance levels: *$p < 0.05$, **$p < 0.01$, ***$p < 0.001$, ***$p < 0.0001$.

reduced the dextran permeability compared with the treatment Baf.

Neuronal validation of autophagy inhibitors

Primary neurons from the embryonic (E) 17.5 mouse cerebral cortex [44] were kept *in vitro* for 7 days before assaying LC3-II by western blot. LC3-II levels increased in response to Baf (20, 60, and 180 nM) (Fig. S6A). Using a published experimental method [45], we incubated neurons in a nutrient-limited medium (nutrient deprivation, ND) and such treatment caused a significant increase of LC3-II levels (Fig. S6B) [45]. NU7441 (10 μM) administered alongside ND dampened LC3-II levels, confirming that this compound causes an early inhibition of the autophagic flux (Figure 5A). Unexpectedly, under ND conditions, both duloxetine and ONC212 (10 μM) increased LC3-II levels (Figure 5B,C). However, ONC212 increased neuronal mortality [46] and was therefore excluded from further analysis (not shown). Poziotinib was ineffective in modulating LC3-II levels in ND-treated neurons (Figure 5D).

An increased swelling of AVs was previously observed in Neuro-2a cells treated with duloxetine with Baf (Figure 4L). We therefore hypothesized that duloxetine might affect the progression of the autophagy flux in neurons, increasing the accumulation of undigested material. To assess this, we measured the protein levels of SQSTM1/p62 (sequestosome 1) [40], using such levels as a functional proxy of the autophagic flux in neurons, as SQSTM1/p62 is itself a target of autophagy. When the autophagic flux increases, SQSTM1/p62 levels decrease as it is degraded by autophagy; in contrast, blocking autophagy progression causes a marked SQSTM1/p62 accumulation in the cell [47–50]. We observed that SQSTM1/p62 levels decreased in ND-treated neurons but remained high in neurons treated with both ND and duloxetine, suggesting that duloxetine impairs progression of the autophagic flux (Fig. S6C).

Cell viability was assessed using MTT (3-[4,5-dimethylthiazol-2-yl]-2,5 diphenyl tetrazolium bromide). We observed a significant increase in MTT absorbance in response to ND treatment. Pharmacological treatments, except for NU7441, did not alter absorbance levels (Fig. S6D). However, the percentage of calcein^{+} PI^{-} (propidium iodide-negative) cells increased with duloxetine compared to ND treatment alone (Fig. S6E). Altogether, these results suggest that duloxetine can impair the autophagic flux in neurons without affecting their survival.

We next assessed whether duloxetine could inhibit autophagy in cells that belong to the BBB. We used primary endothelial cells and astrocytes that we established to study the NVU along with the OGD model. Primary brain endothelial cells were exposed to OGD for 6 and 10 h with or without duloxetine (10 μM) [51]. The OGD treatment produced a slight reduction of LC3-II at both time points, although such reduction did not reach the statistical significance. Similarly, levels of the autophagic marker

SQSTM1/p62 exhibited only minimal variations when compared to control cells suggesting that under these conditions these cells showed a limited activation of the autophagic pathway (Fig. S5H and I). Duloxetine failed to significantly modulate SQSTM1/p62 levels and LC3-II conversion. These results suggest that endothelial cells have low autophagic responsiveness to metabolic stress and the low activation of autophagy is not under the control of duloxetine (Fig. S5H and I).

We next tested LC3-I to II conversion and SQSTM1/p62 protein levels in OGD-treated primary astrocytes (6 and 10 h). The conversion of LC3-I to LC3-II was only slightly modulated by OGD. Similarly, also SQSTM1/p62 levels were slightly increased by 10 h of OGD treatment; duloxetine increased SQSTM1/p62 levels at 10 h suggesting that duloxetine might inhibit the autophagic flux in the cells (Fig. S5J and K).

TRPM2 inhibition affects autophagy

We hypothesized that duloxetine may alter autophagy progression at a stage after the substrate enwrapping in AVs, possibly preventing their degradation. To test this, we aimed to correlate drug treatment with markers of autophagy progression, including SQSTM1/p62. We tracked the lysosome-associated glycoprotein LAMP1 (lysosomal associated membrane protein 1) in naïve Neuro-2a cells treated with OGD, with or without duloxetine (10 μM). MFI levels of $LAMP1^+$ vesicles, scored by confocal microscopy, were increased in cells receiving OGD as well as in cells treated with OGD and duloxetine. While the average number of $LAMP1^+$ puncta did not change in response to these treatments, we observed a significant swelling of $LAMP1^+$ vesicles (Figure 6A,B). Labeling cells with LysoTracker [52] further confirmed that duloxetine induced an enlargement of lysosome likely due to accumulation of undigested material (Figure 6C,D). As expected, OGD reduced the number of $SQSTM1/p62^+$ vesicles, while adding duloxetine to the OGD led to a significant accumulation of $SQSTM1/p62^+$ vesicles (Figure 6E,F).

Since duloxetine inhibits the ADP-ribose – induced TRPM2 (transient receptor potential cation channel subfamily M member 2) channels in neurons [53,54]–which influences Ca^{2+} signaling, redox state, and the lysosomal function – we hypothesized that the TRPM2 inhibition might underlie duloxetine's effect on autophagy.

We assessed by real-time qPCR that *Trpm2* transcripts were expressed by Neuro-2a cells, primary neurons, and cortical explants from healthy mice and mice in which we induced a distal photothrombotic (PT) ischemia (Figure 6G). We observed $TRPM2^+$ vesicles expression in the cytoplasm of Neuro-2a cells (Figure 6H). These vesicles showed a modest colocalization with the Golgi marker GOLGA2/GM130 and with LAMP1 [55], but more pronounced colocalization with the endoplasmic reticulum/ER marker KDEL (Figure 6I). We used two TRPM2 blockers, namely *N*-(pamylcinnamoyl) anthranilic acid (ACA) and 2-aminoethoxydiphenyl borate (2APB) [56,57] to modulate this channel in OGD-treated Neuro-2a cells. Both inhibitors did not exert any toxic effects in Neuro-2a cells at the concentrations that we used to block TRPM2 (Figure 6J). OGD-treated cells diminished the number of $SQSTM1/p62^+$ vesicles, while duloxetine treatment increased this number. Interestingly, the inhibition of TRPM2 using either ACA (20 μM) or 2APB (30 μM) increased the number of $SQSTM1/p62^+$ vesicles, and most importantly co-treatment with duloxetine did not result in a further enhancement of this effect (Figure 6K-N).

Activation of autophagy after ischemic stroke

The autophagic flux was monitored in the somatosensory-motor cortex of mice receiving PT distal ischemia [58,59] by western blotting LC3-II [60]. We compared LC3-II between contralateral and ipsilateral hemispheres of PT mice at 24-, 72-, and 120-h post-stroke induction. The size and the location of PT lesions were evaluated by staining coronal sections with 2,3,5-triphenyltetrazolium chloride (TTC) (Fig. S7A) [61]. In stroked mice, LC3-II protein expression was increased in the ipsilateral, but not in the contralateral hemisphere, when compared to the control (Sham) group at 24 and 72 h after ischemia induction (Fig. S7A-C), confirming that the autophagic flux is enhanced in the CNS following an ischemic insult [17,62–65].

Protective effects of duloxetine on brain injury in the photothrombotic distal model

We next asked whether the selected autophagy inhibitor NU7441 could exert therapeutic effects in stroked mice. NU7441 is a potent inhibitor of PRKDC/DNA-PKcs (protein kinase, DNA-activated, catalytic subunit) [66]. PRKDC/DNA-PKcs is a member of the PtdIns3K-like family which plays a key role in nonhomologous end joining/NHEJ-mediated DNA double-strand break/DSB repair [67]. PRKDC/DNA-PKcs can induce both basal and DNA damage-induced autophagy [68]. NU7441 inhibits PRKDC/DNA-PKcs at the concentration of 14 nM, but it also inhibits PtdIns3K at 5 μM [69,70]; additionally, NU7441 is brain-permeable in mice at the concentration of 5 mg/kg [71]. Ten min after stroke induction, mice received daily intraperitoneal injections of vehicle or NU7441 (5 mg/kg) for up to 3 days (72 h). At the endpoint, they were euthanized and brains stained with TTC. Unfortunately, NU7441 did not reduce the infarct volume in PT mice (Fig. S7D and E).

We next tested duloxetine, initiating the treatment 10 min post-PT induction employing a published administration schema [72]. Female mice received two daily injections of duloxetine (10 mg/kg) to reach a final daily dose of 20 mg/kg (Figure 7A). Three days after stroke induction, the ischemic volume was evaluated on TTC-labeled brain sections. PT mice treated with duloxetine displayed a significant reduction of the infarct volume (Figure 7B,C). Controls only receiving duloxetine did not show any alteration of the gross brain morphology, further confirming the safety of this treatment [72,73] (Figure 7B,C). Using Nissl staining [74], we validated the protective effects of duloxetine assaying the ischemic area in an independent cohort of PT-

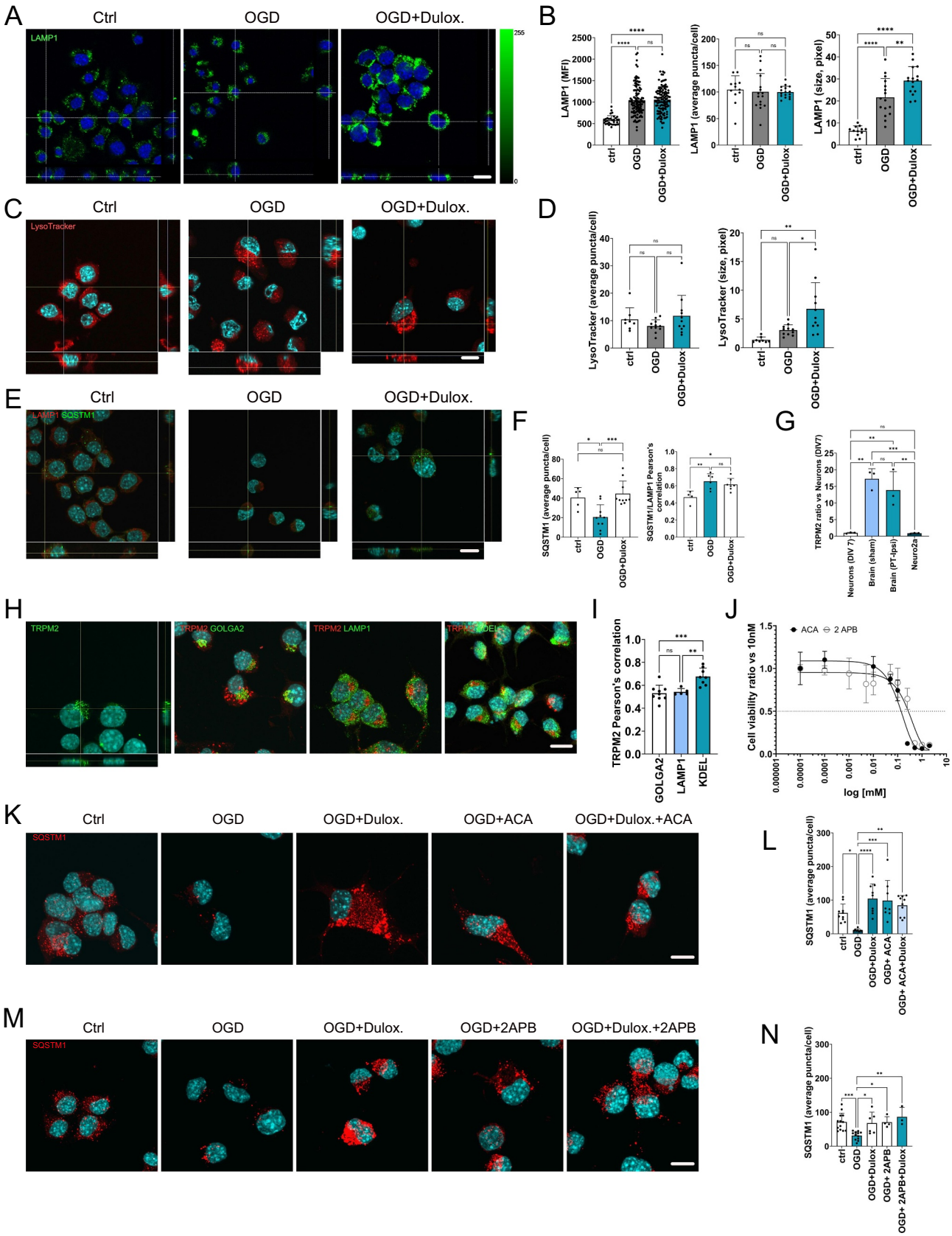

Figure 6. TRPM2 inhibition affects autophagic flux progression. (A) XZ cross-projections of confocal stacks showing Neuro-2a cells exposed to normal culture conditions (Ctrl), OGD (15 h) with or without duloxetine (10 μM), labeled for LAMP1. The epi-fluorescence scale is shown on the right side of the panel. (B) histograms show quantifications of LAMP1 mean fluorescence intensity (MFI) ± SD in gated Neuro-2a cells (dots represent single cells), average LAMP1$^+$ puncta/cell ± SD, and the average size of LAMP1$^+$ puncta ± SD (pixels; each dot represents a single confocal acquisition); $n = 3$ coverslips/condition. (C) XZ cross-projections of confocal stacks showing Neuro-2a cells exposed to normal culture conditions (Ctrl), OGD (15 h) with or without duloxetine (10 μM); cells were incubated with LysoTracker (100 nM) for 40 min before imaging. (D) Histograms show quantifications of the average number and size (pixel) ± SD of LysoTracker$^+$ puncta (each dot represents a single confocal acquisition); $n = 3$ coverslips/condition. (E) XZ cross-projections of confocal stacks showing Neuro-2a cells exposed to normal culture conditions (Ctrl), OGD

induced female mice (Figure 7D,E). Notably, duloxetine was able to preserve brain tissue despite delayed administration after ischemic onset (4 h), suggesting sustained neuroprotective efficacy even the late end of the acute phase. (Fig. S7F). These results confirmed and extended observations raised in a cerebral I/R injury model [75].

The typical stroke patient is elderly, and some indications suggest that these subjects often show comorbidities [76]. We thus compared ischemic lesions in duloxetine- and vehicle-treated one-year-old male mice. Duloxetine (20 mg/kg/day) was administered as above, and the infarct was assessed by Nissl staining in vehicle- and duloxetine-treated mice [74]. We observed that duloxetine was effective in reducing the ischemic area in aged male mice as well (Figure 7F,G).

Both young and aged stroked mice exhibited prominent GFAP (glial fibrillary acidic protein) staining indicating astrocytic activation. Immunolabelling sections for GFAP revealed the presence of a glial scar surrounding the infarct area (Figure 7H,J). Notably, duloxetine reduced the number of activated astrocytes in both groups (Figure 7I,K). The intensity of GFAP staining, as well as the numbers of $GFAP^+$ cells at these cortical regions, appeared lower in duloxetine-treated groups than in mice treated with vehicle (Figure 7H-K).

As we observed in primary neuronal cultures, the conversion of LC3-I to LC3-II was enhanced by duloxetine in cortical explants (Figure 8A-C). We observed that SQSTM1/p62 levels were increased in duloxetine-treated ipsilateral cortical explants (Figure 8D,E) [40]. Duloxetine did not modulate BECN1 (Figure 8D,F), while we observed a reduction of phospho-RPS6KB/p70S6K (ribosomal protein S6 kinase B) in contra- but not in ipsilateral explants (Figure 8G,H).

Given duloxetine's efficacy in reducing the infarct size in young females, we asked whether young male mice also benefited. The week before PT stroke induction, male mice were trained for the balance beam test to assess motor coordination. Baseline performance was recorded 24 h prior to PT stroke induction, and post-stroke assessments were done at 24 and 48 h. Duloxetine treatment slightly increased the time that individual animal spent walking on the narrow beam, reducing the time that they spent crawling on the bar, thus increasing their general locomotion performance (Fig. S7G). The ischemic volume quantified by TTC staining was significantly smaller in duloxetine-treated mice than in vehicle-treated mice (Fig. S7H and I).

Using semi-thin sections, we scored regions flanking the ischemic lesion containing living neurons in and by TEM we scored the number of AVs located in these cells (Fig. S7J and K). The number of AVs in the cytosol was generally small in *bona fide* cortical neurons, probably because LC3 is abundantly expressed in neurites and AVs have a short half-life in brain neurons [77]. However, we observed that the percentage of cells containing at least one AV element was higher in duloxetine-treated mice than in vehicle-treated mice (Fig. S7L).

We hypothesized that an early inhibition of autophagy may confer neuroprotection in stroke. Therefore, we decided to test whether the inhibition of autophagy by 3-MA – a well-established autophagy inhibitor – might recapitulate the protective effects observed in duloxetine-treated animals [78]. Young male mice were intracerebroventricular injected with 3-MA (600 nmol) or with vehicle, 10 min before PT stroke induction. After 48 h, MRI was used to measure the ischemic volume. We observed a significant reduction of the ischemic volume in mice receiving duloxetine compared to vehicle-treated mice (Fig. S7M). By immunohistochemistry we evaluated the spatial expression of CLDN5 (claudin 5), a key structural component of tight junctions [79], in peri-ischemic areas of vehicle- and duloxetine-treated young male mice. CLDN5 levels and distribution were similar between the two groups suggesting that duloxetine can ameliorate stroke injury through mechanisms independent of BBB protection (Fig. S7N).

Altogether these results suggest that early autophagy inhibition in PT mice can exert neuroprotective effects and reduce ischemic brain damage.

Inactivation of autophagy in SLC17A6/Vglut2-expressing neurons protects mice from PT stroke

We next tested an independent approach, not involving pharmacological treatments, to modulate autophagy in PT mice. We crossed mice carrying a floxable *Atg5* allele [80] with mice expressing the ires-Cre cassette downstream of the endogenous *Slc17a6/Vglut2* (solute carrier family 17 member 6) regulatory regions [81]. SLC17A6/Vglut2$^{ires\text{-}Cre/+}$-*atg5*$^{f/f}$ male mice (hereafter *atg5* conditional knockout, *atg5* cKO) and their controls expressing only one floxable *Atg5* allele (*Atg5*$^{f/+}$) were obtained at the expected Mendelian ratio and survived to adulthood,

(15 h) with or without duloxetine (10 µM), labeled for SQSTM1/p62 and LAMP1. (F) histograms show quantifications of the average number of SQSTM1/p62$^+$ puncta ± SD and Pearson's correlation coefficient between SQSTM1/p62 and LAMP1 (each dot represents a single confocal acquisition); $n = 3$ coverslips/condition. (G) RT-qPCR analysis of TRPM2 expression in total mRNA extracts from primary neurons (7 DIV), healthy and ischemic cerebral hemispheres, and Neuro-2a cells ($n = 3$ group, mean ratio vs neurons ± SD). (H) XZ cross-projections of confocal stacks for TRPM2 in Neuro-2a cells; maximal projections of confocal stacks for TRPM2 with either GOLGA2/GM130 (golgi marker), LAMP1, or KDEL (ER marker). Quantification of Pearson's correlations is shown on panel (I); each dot represents a single confocal acquisition; $n = 3$ coverslips/condition. (J) CCK8 assay in Neuro-2a cells (mean absorbance values vs 10 nM ± SD, $n = 6$ wells/condition), treated with ACA or 2APB (10 nM −2 mM); estimated IC_{50} values: ACA = ~370 µM, 2APB = ~790 µM. (K) maximal projections of confocal stacks for SQSTM1/p62 in Neuro-2a cells exposed to normal culture conditions (Ctrl), OGD (15 h), OGD + duloxetine (10 µM), OGD + ACA (20 µM) and OGD + duloxetine (10 µM) + ACA (20 µM). (L) histogram shows quantifications of SQSTM1/p62$^+$ puncta per cell (each dot represents a single confocal acquisition); $n = 3$ coverslips/condition. (M) maximal projections of confocal stacks for SQSTM1/p62 in Neuro-2a cells exposed to normal culture conditions (Ctrl), OGD (15 h), OGD + duloxetine (10 µM), OGD +2APB (30 µM), and OGD + duloxetine (10 µM) + 2APB (30 µM). (N) Histogram shows quantifications of SQSTM1/p62$^+$ puncta per cell (each dot represents a single confocal acquisition); $n = 3$ coverslips/condition. Scale bar: 10 µM. One-way ANOVA followed by Tukey's multiple comparison test was used to analyze data; significance levels: ns, not significant, $^*p < 0.05$, $^{**}p < 0.01$, $^{***}p < 0.001$, $^{***}p < 0.0001$.

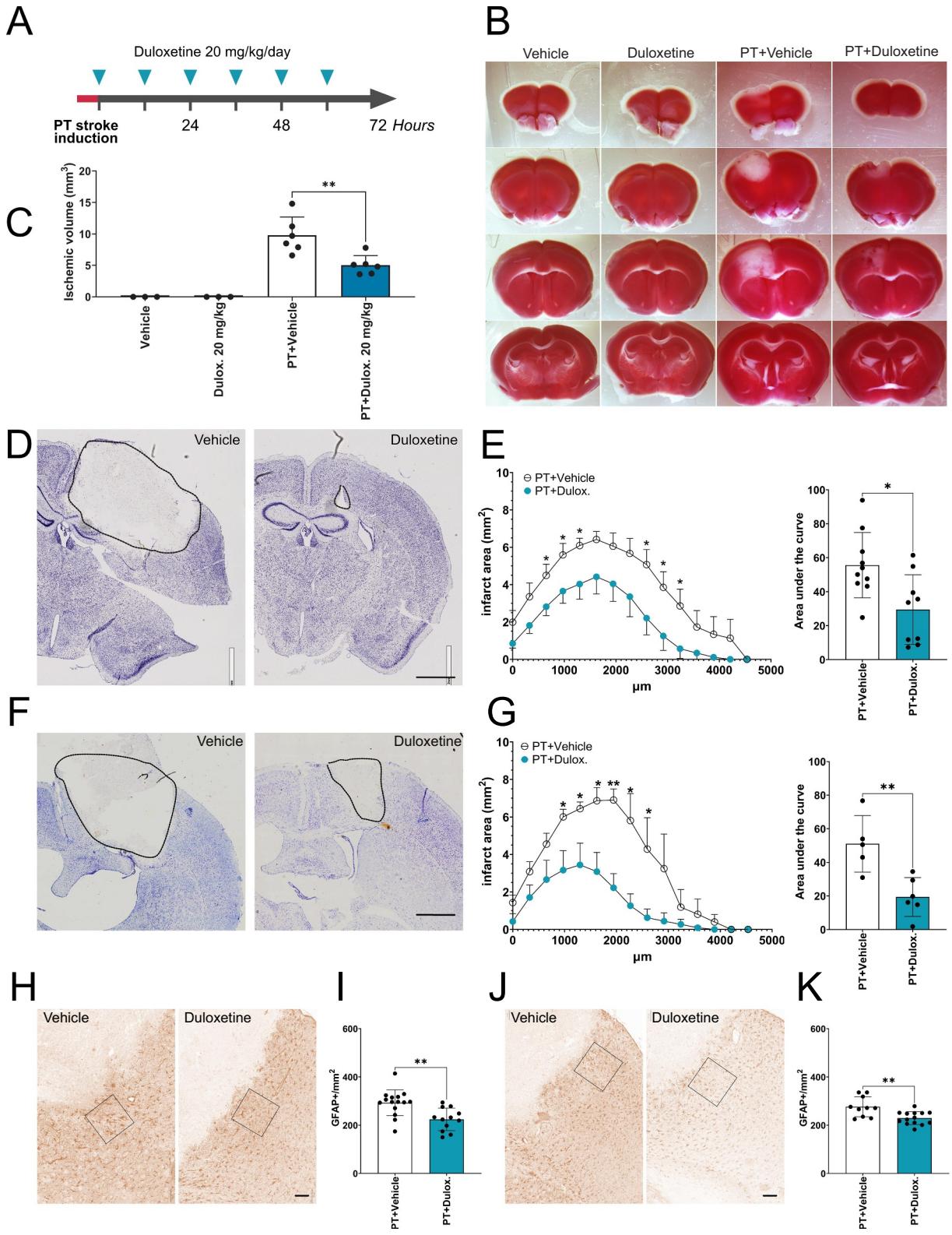

Figure 7. Duloxetine treatment reduces infarct volume. (A) Experimental timeline: mice were treated with duloxetine (10 mg/kg every 12 h) immediately after PT stroke induction. (B) TTC-stained coronal 2 mm-thick brain sections from control mice treated with vehicle or duloxetine ($n = 3$/group), and PT mice ($n = 6$) treated with vehicle or duloxetine (10 mg/kg every 12 h, $n = 6$) and sampled 72 h post-PT stroke induction. (C) the histogram shows quantifications of ischemic volumes (mm^3, mean ± SD). (D) Nissl-stained coronal brain sections from female mice receiving PT stroke induction and treated with vehicle ($n = 10$) or duloxetine (10 mg/kg every 12 h, $n = 9$). (E) the histogram shows quantifications of ischemic area (mm^2) on sections sampled every 300 µm along the anterior-posterior axis. The histogram on the right shows that area under the curve. (F) Nissl-stained coronal brain sections from 1-year-old male mice receiving PT stroke induction and treated with the vehicle ($n = 5$) or duloxetine (10 mg/kg every 12 h, $n = 6$). (G) the histogram shows quantifications of ischemic area (mm^2) on sections sampled every 300 µm along the anterior-posterior axis. The histogram on the right shows that area under the curve. (H and J) GFAP immunohistochemistry on female brains (H) or 1-year-old male brains (J). Quantifications of average $GFAP^+$ cells/mm^2 ± SD in cortical regions flanking the ischemic regions are shown on histograms of (I) and (K). Each dot in panels (I) and (K) represents an individual coronal section used for quantification ($n = 3$ mice per group). Scale bars: 1 mm (B, D, and F); 100 µm (H and J). An unpaired Student's t-test was used to analyze data; significance levels: $*p < 0.05$, $**p < 0.01$.

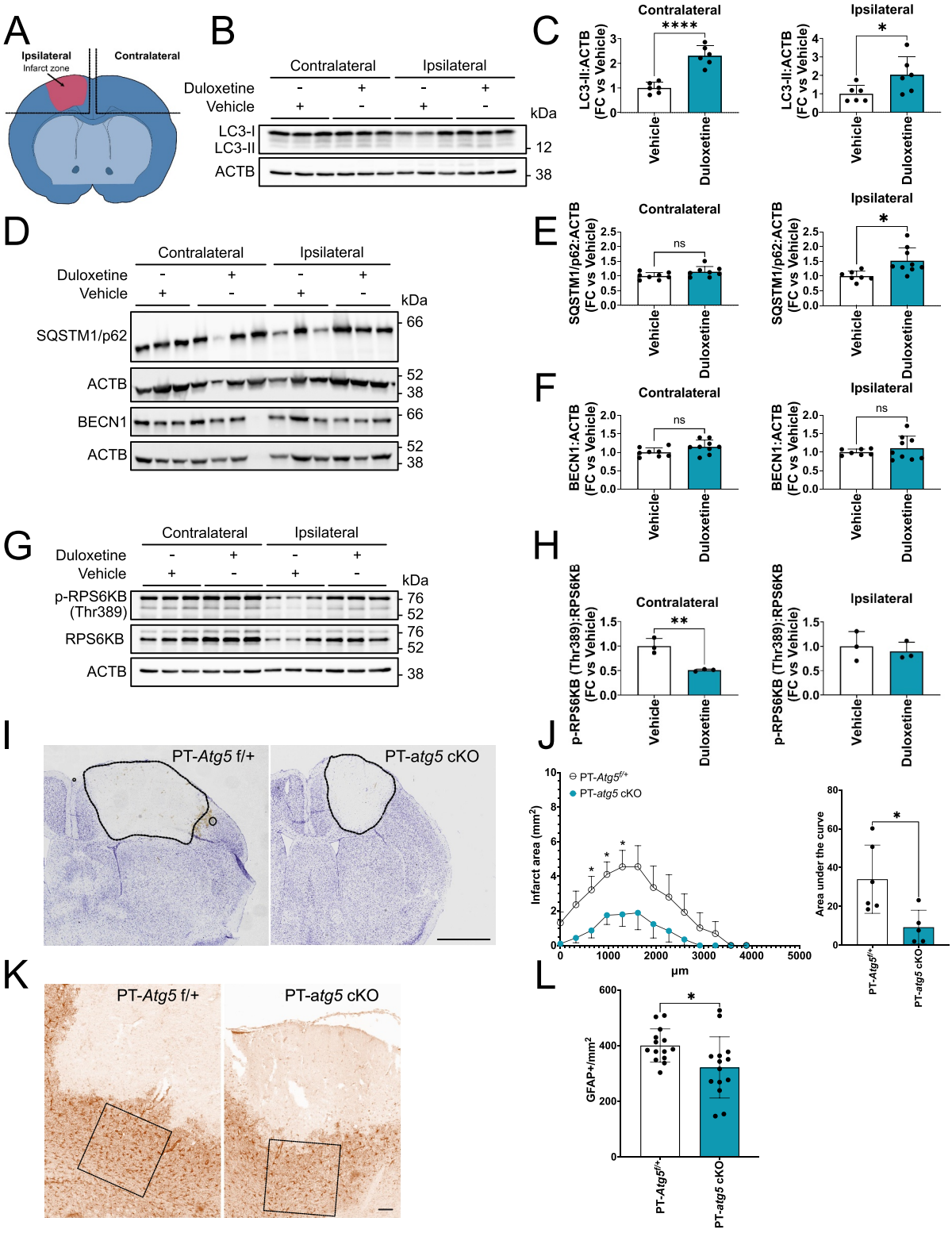

Figure 8. Duloxetine inhibits autophagy in PT stroke brains. (A) schematic of cortical infarct area; dashed lines show regions of the ipsilateral cortex and the contralateral cortex used for western blotting. (B) western blot for MAP1LC3/LC3 and ACTB/β-actin in contralateral and ipsilateral cortical explants from female brains receiving PT stroke induction and treated for 3 days with either vehicle ($n = 6$) or duloxetine (10 mg/kg every 12 h, $n = 6$). (C) histograms show quantifications (mean ratio vs vehicle ± SD). (D) western blot for SQSTM1/p62, BECN1, and ACTB/β-actin in contralateral and ipsilateral cortical explants from female brains receiving PT stroke induction and treated as described above ($n \geq 7$/group). (E and F) histograms show quantifications (mean ratio vs vehicle ± SD) for SQSTM1/p62 (E) and for BECN1 (F). (G) western blot analysis for p-RPS6KB/p70S6K and ACTB/β-actin in contralateral and ipsilateral cortical explants from female brains receiving PT stroke induction and treated as described above ($n = 3$/group). (H) histograms show quantifications (mean ratio vs vehicle ± SD). (I) Nissl staining of coronal sections from *Atg5*$^{f/+}$ ($n = 6$) and *atg5* cKO male ($n = 5$) mice following PT stroke induction. (J) the histogram shows quantifications of ischemic area (mm^2) on sections sampled every 300 μm along the anterior-posterior axis. The histogram on the right shows that area under the curve. (K) GFAP immunohistochemistry on *Atg5*$^{f/+}$ and *atg5* cKO male brains. (L) quantifications of average GFAP$^+$ cells/mm^2 ± SD in cortical regions flanking the ischemic regions, dots show individual sections used for the quantification ($n = 4$/group). Scale bars: 1 mm in (I); 100 μm in (K). An unpaired Student's t-test was used to analyze data; significance levels: ns, not significant, *$p <$ 0.05, **$p < 0.01$, ***$p < 0.001$, ****$p < 0.0001$.

although we observed that mice lacking ATG5 were sometime smaller than their littermate controls (not shown) [80]. Substantial reduction of ATG5 levels in the cerebral cortex of *atg5* cKO mice was revealed by western blot analysis (Fig. S7O). Starting from 3 weeks of age, ATG5 inactivation in NES (nestin)$^+$ progenitors affects motor and behavioral functions in mice [80]. Although it is generally assumed that the constitutive autophagy activity in the healthy brain is quite limited, when compared with other tissues like the liver [82], a long-lasting inactivation of *Atg5* in the CNS increases significantly the accumulation of ubiquitinated proteins in neurons [47]. Therefore, we induced PT stroke in *atg5* cKO mice at the age of 30 days, a time point at which potential side effects deriving from a long-term inactivation of autophagy in excitatory neurons were not observed. Upon PT induction, we labeled sections for MAP1LC3/LC3 by immunohistochemistry. We observed high MAP1LC3/LC3 levels in bona fide neurons flanking the ischemic lesions of control mice, while the MAP1LC3/LC3 immunoreactivity was lower in *atg5* cKO mice (Fig. S7P). The assessment of the ischemic lesion on Nissl-labeled sections from PT mice euthanized 3 days after stroke induction revealed a substantial reduction of the ischemic area in mice lacking ATG5 (Figure 8I,J). Parallel sections labeled for GFAP showed a reduction of GFAP$^+$ cells in *atg5* cKO mice, further corroborating our hypothesis that the early blockage of autophagy can exert protective effects in brain ischemia (Figure 8K,L).

Duloxetine inhibits autophagy in human 3D brain organoids

Human brain organoids were differentiated from neural precursor cells (NPCs) engineered with SOX10 (SRY-box transcription factor 10) lentiviral vectors to achieve oligodendrocyte maturation in culture [83]. After 8 weeks, they were immunolabeled for GFAP, MAP2 (Microtubule Associated Protein 2), and PLP1 (Proteolipid Protein 1), while SOX10-GFP expression was checked by autofluorescence. Representative images show that our cellular model is composed of multiple cell types present in the human brain, such as differentiated neurons (MAP2$^+$), astrocytes (GFAP$^+$), and oligodendrocytes (PLP1$^+$), as well as SOX10 pan progenitors (Fig. S8A and B).

As expected, human brain organoids exposed to OGD for 24 h significantly enhanced HIF1A/HIF-1α levels and reduced ULK1 phosphorylation levels at Ser 757, suggesting that OGD might enhance the autophagic flux in brain organoids (Fig. S8C and D). Parallel cultures were treated with OGD with or without duloxetine (10 μM) for 24 h. The autophagic flux was examined by immunoblotting for MAP1LC3/LC3 and SQSTM1/p62 [37,50]. In this experimental setting, the LC3-II:ACTB/β-actin ratio was increased by the OGD treatment, whereas SQSTM1/p62 levels were decreased. Adding duloxetine to the medium slightly but significantly decreased LC3-II while increased SQSTM1/p62 (Fig. S8E and F). The OGD treatment increased the expression level of ATG5, which is involved in upregulation of the autophagic flux [84]. Interestingly, duloxetine treatment dampened such activation (Fig. S8G). We observed that OGD-treated organoids increased the level of cleaved CASP3 (caspase 3; cCASP3), although this upregulation was not statistically significant. However, duloxetine counteracted this upregulation, bringing cCASP3 levels close to the baseline levels observed in untreated organoids (Fig. S8H). Taken together, our results suggest that duloxetine plays a significant role in attenuating autophagic flux activation in human brain organoids following OGD, highlighting its potential as a neuroprotective agent in ischemic conditions.

Discussion

The complexity of stroke pathobiology poses significant challenges to the development of new treatments. To date, recombinant PLAT (plasminogen activator, tissue type) is the only FDA-approved drug for ischemic stroke [85–87]. However, a relatively small percentage of patients benefit from thrombolytics due to the narrow therapeutic time window [88]. Thus, there is an urgent need for new therapeutic strategies to foster neuroprotection, reduce infarct volume, and minimize reperfusion damage.

Autophagy, a cellular adaptive response, counters nutrient depletion and is generally regarded as protective, contributing to neuronal homeostasis restoration [89]. However, under specific circumstances, autophagy can contribute to cell death [90]. In brain ischemia, autophagy is linked to early pathological events, activated by the loss of oxygen and nutrients [91,92]. In rodent stroke models, autophagy activation is often seen as an adaptive response that protects neurons, although whether its modulation after stroke is beneficial remains a matter of debate [65,93,94].

Across brain injury models like traumatic brain injury (TBI) and ischemia, severity appears to dictate whether autophagy mediates protection or exacerbates damage. In TBI, mild injuries tend to activate autophagy in a protective manner, while severe injuries often result in impaired flux and autophagic cell death or dysfunction [95]. In brain ischemia, prolonged or severe stress can shift autophagy from a beneficial adaptive process to a maladaptive one, especially when autophagic flux is blocked, leading to accumulation of damaged cellular components.

Neuroprotective effects of autophagy activation have been reported in different experimental settings [96], particularly in preconditioning models. For example, autophagy modulators that either enhance or inhibit autophagic flux have been shown to influence outcomes, either enhancing neuroprotection or diminishing the protective effects of preconditioning, respectively [97,98]. However, there are several studies showing that autophagy activation exacerbates neurotoxicity in stroked brains [17]. We observed that the blockade of autophagy PT brains by 3-MA (a PIK3C3/VPS34 [phosphatidylinositol 3-kinase catalytic subunit type 3] inhibitor) reduces the infarct size, confirming data derived from transient middle cerebral artery occlusion/tMCAO models [99].

In this study, we screened a library of small molecules to identify novel modulators of the autophagic flux that can be used in mammals. We used a combination of approaches, starting with virtual screening to identify drugs active in the

mammalian CNS. The computational analysis of each molecule was conducted by evaluating the distribution of eight properties, including the Lipinski's Rule-of-Five [100]. Evaluating the drug-likeness of a large set of molecules using traditional approaches is often a complex and resource-intensive process [101]. Indeed, identifying promising leads is usually time-consuming and expensive. Computational methods, however, significantly streamline this process, facilitating drug-like assessments [102]. In our analysis, a CNS-drug likeness prediction strategy eventually resulted in the exclusion of 5941 compounds, narrowing the focus to 898 promising candidates for further biochemical evaluation. It is important to note that over 350 of these selected molecules are FDA-approved, with well-documented information about their toxicity, formulation, pharmacology, and potential side effects. This effort aligns with a classical drug repurposing strategy, which, as demonstrated during the recent COVID-19 pandemic, offers the advantage of rapidly redirecting an existing molecule for new therapeutic applications [103].

To establish the primary screening assay, we used Neuro-2a cells to monitor LC3 turnover, a robust approach widely used to track autophagy progression. Following LC3-II conversion, autophagosomes fuse with lysosomes, leading to the degradation of proteins by hydrolases [24,37,104,105]. To track autolysosome formation, we used a plasmid encoding a super-ecliptic pHluorin-mKate2-tagged human LC3 chimera (PK-hLC3) [24]. Super-ecliptic pHluorin is a pH-sensitive GFP variant that increases the sensitivity of the assay by almost completely quenching at pH < 6.5, providing a reliable readout of autophagosome-lysosome fusion [24]. Establishing a stable Neuro-2a cell clone expressing PK-hLC3 further reduced variability associated with transient transfection procedures.

We quantified pHluorin fluorescence levels by flow cytometry [28] and used OGD to mimic hypoxia and nutrient deprivation-two key conditions observed in stroke [106]. To enhance the assay's interpretative power, we included torin-1 (a well-known autophagy inducer) and Baf (a well-known late-stage autophagy inhibitor) as controls. Although this could in principle allow us to distinguish between torin-like molecules (putative autophagy inducers) and Baf-like compounds (putative autophagy inhibitors), we acknowledge that the assay cannot reliably differentiate late-stage autophagy inhibitors from early-stage inhibitors, as both could lead to increased pHluorin levels compared to OGD controls. This limitation arises because late-stage inhibitors cause autophagosome accumulation in the cytoplasm, while early-stage inhibitors block the process upstream, preventing the 25% pHluorin fluorescent signal decrease induced by OGD, which we included to mimic stroke conditions.

Quality control analysis and hit selection utilize both control-based and non-control-based normalization approaches. The former considers in-plate positive and negative controls but is susceptible to well variability. The latter assumes that most samples are inactive, reducing random variability among wells [107]. To minimize potential off target activity, each compound was tested at 1 μM in triplicate. We obtained 22 compounds that significantly modulated autophagy under OGD-reperfusion conditions. The list of selected compounds included the autophagy inhibitors ULK-101 and quinacrine [34,35], which served as controls and were not further investigated.

Selected molecules were validated by monitoring LC3-II turnover in naïve Neuro-2a cells under basal conditions and upon treatment with each selected compound, both in the presence and absence of saturating levels of Baf [40]. Results from this validation phase confirmed six compounds, which were also tested for their dose-response effects, and analyzed by TEM.

The selected molecules were then tested on primary neuronal cultures subjected to ND, a protocol mimicking the nutrient loss experienced by ischemic neurons [45]. Among the tested compounds, the DNA-PK inhibitor NU7441 [66] emerged as the most potent early-stage inhibitor of the autophagy flux, effectively blocking autophagy in both Neuro-2a and primary neurons. None of the tested autophagy inducers significantly enhanced autophagic flux in primary neurons, nor did they exhibit a consistent dose-response relationship in Neuro-2a cells.

The reperfusion phase is critical for rescuing neuronal cells but is also associated with additional neuronal damage termed "reperfusion injury." This phenomenon involves the production of reactive oxygen species (ROS), which can damage DNA [108]. DNA repair of double-strand breaks in mammalian cells is primarily achieved via non-homologous end joining, a process involving several proteins, including DNA-PK. Notably, protracted ischemia in the rabbit spinal cord affects the expression of PRKDC/DNA-PKcs, whereas shorter ischemic episodes do not [109]. Among the PRKDC/DNA-PKcs targets, TP53/p53 is activated in response to DNA damage and this activation can lead to either cell cycle arrest, allowing repair, or the induction of TP53-dependent apoptosis [110]. Moreover, PRKDC/DNA-PKcs is a member of the phosphatidylinositol-3 kinase-like (PIKK) family, also containing MTOR [111] NU7441, in addition to inhibiting PRKDC/DNA-PKcs, can modulate other kinases belonging to PIKK family at low micromolar concentrations [112]. Moreover, PRKDC/DNA-PKcs phosphorylates PRKAG1/AMPKγ1 (protein kinase AMPK-activated non-catalytic subunit gamma 1), indirectly regulating the activation of autophagy [68]. The complex interactions of NU7441 with multiple targets may yield opposing and unpredictable effects on autophagic flux in the brain. We established that NU7441 is a potent early autophagy inhibitor *in vitro*, therefore we tested this compound in the PT mouse model, initially established in 1977 [113] and later improved by Watson [58], observing that it fails to reduce the ischemic infarct volumes. This outcome might be explained by the complex pathological cascades triggered during stroke, including Ca^{2+} overload, microglial activation, and infiltration of immune cells producing ROS and nitric oxide (NO), which in turn affect the DNA homeostasis in neurons [114]. Inhibiting PRKDC/DNA-PKcs in stroked brains may sensitize neurons to DNA damage and oxidative stress, as seen in hippocampal neurons lacking PRKDC/DNA-PKcs activity (SCID mice) [115].

Duloxetine treatment of PT mice, at a previously established dose (20 mg/kg/day) [116], showed a reduction of the ischemic lesions by approximately 50%. This reduction was consistent across males, females, and one-year-old animals.

Moreover, delayed administration of duloxetine following PT induction retained protective efficacy. Duloxetine is a SNRI clinically used to treat depression, anxiety, and chronic pain [117–119] and in the range between 30 and 60 mg/day it is generally considered safe for treating central poststroke pain in patients [120–122]. However, mild side effects such as somnolence, nausea and dizziness have been observed. Previous studies in ischemic/reperfusion models demonstrated that administering duloxetine before reperfusion reduces the ischemic volume [75]. Similarly, another study showed that the pretreatment of gerbils with duloxetine protects CA1 neurons in a transient global cerebral ischemia protocol, reducing microglial activation and astrogliosis [53].

Notably, under Baf treatment we noticed that duloxetine inhibits autophagosome formation dampening LC3-II levels in Neuro-2a cells. In neurons exposed to ND, duloxetine increased LC3-II levels; however, SQSTM1/p62 also accumulated, which is a hallmark of impaired autophagic flux. Therefore, under ischemic or neurodegenerative stress conditions, duloxetine appears to impair autophagic degradation or lysosomal clearance, resulting in the accumulation of both LC3-II and SQSTM1/p62. Since Baf inhibits autophagosome – lysosome fusion by neutralizing lysosomal pH, it acts at the terminal stage of the autophagic process and therefore cannot induce the formation of new autophagic vesicles. OGD and ND stressors stimulate the autophagic flux, increasing rates of autophagosomes formation and the accumulation of LC3-II in the cytoplasm. However, if cells cannot complete the recycling of materials enclosed in autophagic vesicles, the blockage of autophagic degradation leads to the accumulation of both LC3-II and SQSTM1/p62. Besides its known inhibition of serotonin and noradrenaline transporters, duloxetine also blocks TRPM2 (transient receptor potential cation channel subfamily M member 2) channels at low micromolar concentrations. The TRPM2-Ca^{2+} -CAMK2-BECN1 signaling cascade, which is activated following ischemic injury, has been implicated in the regulation of autophagy. Thus, by inhibiting TRPM2, duloxetine may attenuate autophagic activation under ischemic conditions [123]. This hypothesis is further supported by evidence showing that two well-characterized TRPM2 inhibitors induce the accumulation of SQSTM1/p62 in OGD-treated cells. However, the physicochemical properties of these compounds preclude their application in *in vivo* models.

Duloxetine blocks persistent late Nav1.7 Na^+ currents in neurons [124], although there is no direct evidence linking these channels to brain ischemia. Treatment with duloxetine significantly attenuated neuronal cell death in the CA1 region of the hippocampus of rats subjected to chronic cerebral hypoperfusion, possibly by modulating the AKT-MTOR-RPS6KB signaling pathway, which contributes to autophagy inhibition [125]. Therefore, we cannot exclude the possibility that the autophagy inhibition observed in PT mice also reflects activation of the AKT-MTOR-RPS6KB pathway.

We also observed that duloxetine can modulate SQSTM1/p62 in human brain organoids, a multicellular system characterized by different cell types, including precursor cells, oligodendrocytes and neurons at different maturation stages, and astrocytes. According to the literature, murine TRPM2 is mainly expressed by neurons [126], astrocytes, and microglia [127,128], while human TRPM2 expression has been confirmed by scRNAseq in neurons, microglia, and CNS macrophages, with barely detectable levels in astrocytes and oligodendrocytes (Human Protein Atlas: TRPM2 Expression). Single cell-RNAseq data from our human brain organoid model confirmed TRPM2 expression only in differentiated neurons, which represent approximately 20% of the total cell population. This limited receptor distribution likely explains the partial autophagy inhibition observed, as autophagy remains active in most cells lacking TRPM2 expression.

The potential of certain antidepressants, such as duloxetine, sertraline, fluoxetine, or indatraline, to act as autophagy modulators is not new, although molecular mechanisms are still under investigation [129–131]. Results from our molecular screening indicate that duloxetine is an autophagy inhibitor *in vitro*, and we hypothesize that, acting on TRPM2, it can reduce the autophagic flux in post-stroke neurons. An early inhibition of autophagy in stroke has been considered protective, and we extended this finding on PT mice by injecting the brain with 3-MA before inducing the PT model.

We also used transgenic mice carrying a floxable *Atg5* allele to inhibit autophagy. These transgenic mice were crossed with mice expressing the Cre recombinase in excitatory neurons. We observed a significant reduction in the ischemic volume in double transgenic mice subjected to the PT model, reinforcing the hypothesis that the abrupt activation of autophagy after ischemia affects neuronal cell survival. However, it is important to note that a long-lasting CNS inhibition of autophagy is detrimental, inducing a neurodegenerative phenotype [80]. For this reason, we used only young transgenic mice carrying the conditional inactivation of *Atg5* in excitatory neurons. In this setting, we did not see any pathological outcomes resulting from the suppression of autophagy. We examined the impact of *Atg5* inactivation on mice sampled 3 days after PT induction. Nonetheless, we cannot exclude that inhibiting autophagy for weeks might result in an opposite phenotype.

In summary, our results suggest that early administration of duloxetine exerts neuroprotective effects in experimental models of distal cerebral ischemia, reducing neuronal death and improving functional outcomes.

Materials and methods

Compounds

The cherry-pick library containing 898 compounds (384-well, L2000-Z382759-30 µL) was assembled by Selleckchem. Torin-1 (4247) and bafilomycin A_1 (1334) were purchased from Tocris Bioscience. Puromycin (P8833) and 3-methyladenine (M9281) were sourced from Sigma-Aldrich. For *in vitro* validation experiments, bepridil hydrochloride (HY-16952A), darapladib (HY-10521), ONC212 (HY-111343), duloxetine-HCl (HY-B0161A), bedaquiline fumarate (HY-14881A), closantel (HY-17596), and Dp44mT (HY-18973) were purchased from MedChemExpress; WAY-331960 (*p*-425440429), WAY-326275 (*p*-34884134), WAY-656627 (*p*-6984125), WAY-348105 (*p*-605854424), WAY-640783 (*p*-486113558), and

PTC-028 (*p*-608273002) were obtained from Mcule; NU7441 (S2638), chlorpromazine (S5749), MK-8745 (S7065), poziotinib (S7358), and MI-2 (S7429) were purchased from Selleckchem. *N*-(pamylcinnamoyl) anthranilic acid (A8486), and 2-aminoethoxydiphenyl borate (D9754) were obtained from Sigma-Aldrich. *In vivo* validation experiments were performed using NU7441 (S2638) and duloxetine HCl (S2084) from Selleckchem.

In silico *screening procedures*

The list of compounds included in the Bioactive Compound Library-I (Selleckchem, L1700) was *in silico* analyzed and screened according to a specific set of functional parameters. *In silico* analysis was conducted using the QikProp absorption, aistribution, metabolism, and excretion/ADME prediction tool (Schrödinger, LLC, New York), which uses an algorithm based on the correlation between experimentally determined properties and Monte Carlo simulations. Molecules underwent the first prioritization round based on pharmaceutically relevant drug metabolism and pharmacokinetics (DMPK) properties listed in Table 1. After the first analysis, 1927 molecules underwent a second prioritization round. Compounds ranking was performed using a linear function to assign a score to the most relevant properties identically weighted. CNS, QPPMDCK, and QPlogBB descriptors were selected to rank the compounds. We obtained 898 compounds that were subjected to functional screening on 7B11 cells, a clone that we obtained from a screening on Neuro-2a cell line.

Cell culture

The Neuro-2a cell line was obtained from the American Type Culture Collection (ATCC, CCL-131™). Cells were plated on culture dishes or multiwell plates and maintained in Dulbecco's modified Eagle's medium (DMEM; Gibco, 11,965,084) supplemented with 10% fetal bovine serum (FBS; Corning, F7524) and 1% penicillin-streptomycin (Gibco, 15,140–122). Cells were grown in a humidified 5% CO_2 atmosphere at 37°C. To generate a stable cell line expressing a proxy for autophagy monitoring, we transfected Neuro-2a cells with the pEX-PK-hLC3 plasmid (Addgene, 61,458; deposited by Isei Tanida) [24] following Lipofectamine LTX (Invitrogen, A12621) manufacturer's protocol. Twenty-four hours post-transfection we applied antibiotic selection with 4.5 µg/mL puromycin. The culture medium was refreshed every 2–3 days. After a week, the resistant bulk culture was seeded in a 96-well plate, to run a limiting dilution cell selection. Single clones were selected by the aid of inverted microscope, grown in the selection medium for 14 days, and periodically inspected for morphology and fluorescence intensity. Selected clones were expanded and cryopreserved for further analysis. Upon selection, clone 7B11 was used for the primary screening.

Primary cortical neurons were obtained from E17.5 C57BL/6 cerebral cortices and used at day *in vitro* (DIV) 7 according to our published protocol [44]. Embryonic brains were dissected under sterile conditions in cold Hanks' Balanced Salt Solution (HBSS; Sigma-Aldrich, 55037C) supplemented with 0.6% D-(+)-glucose (Sigma-Aldrich, G8270) and 5 mM HEPES (Gibco, 15,630–080). After dissection, single cortices were gently triturated to loosen up the tissue. Cells were mechanically dissociated and resuspended in the dissection medium, followed by centrifugation at 100 x *g* for 5 min. Cells were plated on cell culture treated multiple-well plates or HNO_3-treated glass coverslips (VEMI, Zeus 13 mm), both coated with 0.2 mg/mL poly-L-lysine (Sigma-Aldrich, P2636) and 10 µg/mL mouse LAMA (laminin; Sigma-Aldrich, L2020). Cells were maintained in Neurobasal-A medium (Gibco, A2477501) supplemented with 2% B27 (Gibco, 17,504), 1% L-glutamine, 0.6% D-glucose, and 5 mM HEPES. Twenty-five percent of the culture media was refreshed every 2–3 days, and cells were kept at 37°C with 5% CO_2 until DIV7. Nutrient deprivation induction on primary neuronal cultures was adapted from a previously described protocol [45]. Briefly, primary cortical neurons from E17.5 embryos were plated in the complete Neurobasal-A medium at a density of 2.2×10^5 cells/well in 12-well multiple-well plates (Costar, 3513). At DIV7, the complete medium was replaced with nutrient-limited media (DMEM alone). For autophagy modulation studies, neurons were cultured for 15 h in the presence or absence of selected compounds at the final concentration of 10 µM.

Neural precursor cells (NPCs) were derived from human fibroblasts we sampled from a healthy donor, according to the ethical committee of the San Raffaele Hospital (Milan, Italy) (BancaINSpe-INSPE1178). Written consent was obtained from all subjects involved in this research. Differentiation from induced pluripotent stem cells (iPSCs) to NPCs has been performed according to Reinhardt's protocol [132]. NPCs were then infected with a lentiviral vector encoding the human SOX10 and GFP under the control of a doxycycline-inducible promoter. GFP^+ NPCs were sorted and expanded in Matrigel-coated flasks in N2-B27 medium, containing equal parts of Neurobasal (Gibco, 21,103–049) and DMEM-F12 medium (Gibco, 11,090–081) with 1:100 B27 lacking vitamin A (Gibco, 12,587–001), 1:200 N2 (Gibco, 17,502–048), 1% penicillin-streptomycin (Thermo Fisher, 15,-140–122), 1% glutamine, supplemented with 3 µM CHIR (Tocris Bioscience, 4953), 1 µM SAG (Millipore, 566,660-1 m), 150 µM ascorbic acid. The human brain organoids were generated as described [83]. Briefly, at 100% confluency, NPCs were enzymatically detached and counted. 2.5×10^6 cells per well were plated in uncoated ultra-low adhesion 6 well-plates in N2-B27 medium under constant gyratory shaking (88 rpm). After 24 h, the medium was changed to glial induction medium (100% DMEM-F12, 1:100 B27 lacking vitamin A, 1:200 N2, 1% penicillin-streptomycin, and 1% L-glutamine), supplemented with 10 ng/mL triiodo-L-thyronine (T3; Sigma-Aldrich, T6397), 10 ng/mL rHsPDGF (Pepro Tech, 100-13A), 10 ng/mL rHsNT3 (Pepro Tech, 450–03), 1 µM SAG, 10 ng/mL IGF1 (Pepro Tech, 100–11), 200 µM ascorbic acid, and 1 µg/mL doxycycline (Sigma-Aldrich, D3447) from day 1 to day 3. From day 5 till the end of the differentiation protocol, medium was replaced with glial differentiation medium: 100% DMEM-F12, 1:100 B27 lacking vitamin A, 1:200 N2, 1% penicillin-streptomycin,

and 1% L-GLS (glutaminase), supplemented with 60 ng/mL T3, 10 ng/mL rHsNT3, 10 ng/mL IGF1, 200 µM ascorbic acid, and 100 µM cyclic AMP analog (dbcAMP; Sigma-Aldrich, D0627). 1 µg/mL doxycycline from day 5 until day 14, while 0.01 µg/mL human recombinant GDNF (Pepro Tech, 450–10) and BDNF (StemCell Technologies, 05270) were added to the culture medium from day 14 till the end of the differentiation protocol. Half of the medium was changed three times a week. Cultures were maintained at 37°C, 5% CO_2 under constant gyratory shaking (88 rpm) for 8 weeks.

Primary brain endothelial cells were isolated from the mouse brain using our published procedure [133]. Briefly, mice were euthanized, and brains were dissected. Meninges and choroid plexus were surgically removed. Cortices were isolated and finely minced with a scalpel on ice and digested with 3.5 mg/mL collagenase/dispase (Roche, 11,097,113,001) for 30 min at 37°C in continuous rotation. After dissociation, 10 mg/mL DNAse (Sigma-Aldrich, DN25-1 G) was added, samples were pipetted to obtain a homogeneous solution. Myelin cell debris and erythrocytes were removed by stratification over a 22% Percoll solution (GE Healthcare, 17,089,101). Samples were centrifuged for 20 min at 600 x *g* at 4°C, no brake. Cells were seeded into 0.1 mg/mL rat tail collagen type I (lower viscosity; Cultrex, 354,236)-coated wells, and cultured at 37°C, 5% CO_2 with saturated humidity in EBM-2 medium (Lonza, CC-3156) supplemented with 2% heat-inactivated fetal bovine serum (Lonza, CC-4101A), 1% penicillin-streptomycin (Lonza, BW09-757F), 1% chemically defined lipid concentrate (Invitrogen, 11,905,031) and EGM-2 SingleQuots (Lonza, CC-31626). After 3 days of puromycin selection (4 µg/mL; Sigma-Aldrich, SP8833) in complete medium, medium was changed every other day.

Primary mouse astrocytes were isolated from the mouse brain using our published protocol [134]. Brains were extracted from new-born C57BL/6J wild type mice, meninges and choroid plexus were surgically removed, cortices were mechanically dissociated and digested with a buffer containing 2.5% trypsin (Lonza, BE17-160E), 10 mg/mL DNase and Hanks' Balanced Salt Solution medium (Gibco, 12,350,039) for 30 min at 37°C in agitation. Mixed cultures were seeded on tissue culture flasks coated with 0,1 mg/mL poly-D-lysine (Sigma-Aldrich, P4707). Cells were maintained at 37°C, 5% CO_2/saturated humidity, in minimum essential medium with Earle's salts (Gibco, 42,360–081) supplemented with 10% heat-inactivated FBS (MICROGEM Laboratory Research, S1860-500) and 1% penicillin-streptomycin (Lonza, BW09-757F), glucose 0.6% (Sigma-Aldrich, G7021), 1% sodium pyruvate 2 mM (Lonza, BW13-115E), 1% UltraGlutamine supplement (Lonza, BEBP17-605E). Upon shaking at 230 rpm for 45 min in medium containing minimum essential medium with Hanks' salts supplemented with 10% heat-inactivated fetal bovine serum and 1% penicillin-streptomycin, glucose 0.6%, 1% sodium pyruvate 2 mM (Lonza, BW13-115E), 1% UltraGlutamine supplement the remaining adherent cells were detached and used for the experiments.

Oxygen-glucose deprivation

OGD experiments were performed on 7B11 cells or on parental Neuro-2a cells plated in complete DMEM supplemented with 4.5 µg/mL puromycin, at a density of 1.2×10^5 cells/well in 12-well multiple-well plates (Costar, 3513) and grown for 24 h. Immunofluorescence experiments were run on Neuro-2a cells plated on poly-lysine (0.2 mg/mL) coated glass coverslips. To induce OGD, the complete medium was replaced by deoxygenated, serum-free, glucose-free DMEM (Sigma-Aldrich, D5030) supplemented with 3.7 g/L $NaHCO_3$ and 1% penicillin-streptomycin, and cells were exposed to a hypoxic atmosphere (1% O_2, 5% CO_2, 94% N_2) in a controlled-oxygen workstation (SCI-tive, Baker Ruskinn). Individual molecules were tested in OGD conditions at a final concentration of 1 µM, for 15 h. Depending on the diluent used to resuspend individual molecules, controls were established using DMSO or water.

7B11 or parental Neuro-2a cells were treated with torin-1 (250 nM, 24 h) and/or Baf (200 nM, 15 h) [135] to achieve controls that were alternatively included in each experiment. Both parental Neuro-2a and 7B11 cells were kept in culture for no more than four *in vitro* passages.

Human brain organoids were resuspended in GDM without glucose and treated with (1% O_2, 5% CO_2, 94% N_2) in the controlled-oxygen workstation (SCI-tive, Baker Ruskinn) for 24 h.

Primary glia cells and primary endothelia cells plated on 12-well multiwell plates (Costar 3513) were exposed to preconditioned Neurobasal medium containing supplements but the glucose. Cells were incubated in in the controlled-oxygen workstation (1% O_2, 5% CO_2, 94% N_2) for 6 and 10 h before protein extraction.

LysoTracker Red (Thermo Fisher, L7528) was prepared at the final concentrations of 100 nM, incubated for 40 min on both OGD-treated cells and controls at the end of the treatment. Cells were washed with 1X PBS, fixed in 4% paraformaldehyde (PFA; Sigma-Aldrich, P6148) and immediately imaged.

Flow cytometry

At the end of the OGD protocol, 7B11 cells were processed in normoxic conditions and prepared for flow cytometry. Briefly, living cells were detached with 0.05% Trypsin-EDTA (Gibco, 25,300,120), transferred to a 96-well multiple-well plate (V-bottom), centrifuged at 300 ×for 5 min at 4°C, and washed with cold PBS. After washing, cells were stained with Zombie NIR Fixable Viability kit (Biolegend, 43,105) for 20 min at 4°C. Fluorescence signals were acquired on Cytoflex S flow cytometer (Beckman Coulter), in a semi-automated setting. Upon acquisition, events were gated on single and viable cells. For each sample, 1×10^7 living cells were acquired and analyzed with FlowJo software (BD Biosciences).

MTT and CCK8 assays

To test the drugs toxicity on primary neuronal cultures and Neuro-2a cells, we plated cells on 96 multiwell (neurons: 4 x10^4/well; Neuro-2a: 15x10^4/well). After drug treatment for 15 h, cells were washed, treated with MTT working solution 0.5 mg/mL and then incubated at 37°C for 3 h. After incubation time reaction was stopped with DMSO and measured at

570 and 650 nm wavelength. DMSO-treated wells were loaded and used as control.

CCK8 assay was done incubating Neuro-2a cells with increasing amounts of ACA (Sigma-Aldrich, 99,196–74-74) or 2-APB (Sigma-Aldrich, 524–95-8). Fifteen hours later, cells were incubated with 10 µL of the CCK8 reagent (Sigma-Aldrich, 96,992) for 2 h before measuring the absorbance at 570 nm.

Calcein assay

Each drug was also tested for neuronal vitality after 15 h of treatment, and cells were immediately stained with propidium iodide (PI) to stain apoptotic cells (1 mg/mL), calcein to stain membrane-permeable live cells (0.1 mg/mL), and Hoechst (1 mg/mL) to measure the total cells present in the region of interest. Cells were incubated for 15 min at 37°C protected from light and then immediately acquired at the microscope.

Real time PCR

Total RNA was extracted from cultured cells and brain explants using RNeasy mini (Qiagen, 74,104 RNeasy mini kit 50). cDNA was synthesized from 0.5–1.0 µg total RNA using Superscript IV kit (Invitrogen, 18,090,200) with random hexamers following the manufacturer's protocol. Real-time PCR was performed on a (QuantStudio 5, Applied Biosystem) using SYBR Green Master Mix (EvaGreen; Bio-Rad, 1,725,124) in 20 µL reactions with the following primers: *TRPM2* F: 5' accccgcctgcacatgcaccatg 3,' *TRPM2* R: 5' gatcgcttatagagggaccggagg 3,' *H3* F: 5' gtgaagaaacctcatcgttacaggcctggtac3' and *H3* R: 5' ctgcaaagcaccaatagctgcactctggaagc 3.'

Animals

Experiments were performed using young C57BL/6N 8–10-weeks old mice of both sexes (total number of females used in the study $n = 68$, average body weight:18–22 g; total number of males used in the study $n = 79$, average body weight: 22–26 g) and one year old C57BL/6N males (total number of mice used in the study $n = 11$, average body weight: 28–34 g), (Charles River Laboratories). Mice were maintained at San Raffaele Hospital mouse facility (Milan, Italy) under specific pathogen-free and temperature-controlled conditions and a standard 12-h light-dark cycle with food and water *ad libitum*. Experimental procedures were approved by the Institutional Animal Care and Use Committee (IACUC No. 692, 798, and 1198), and all efforts were made to minimize animal suffering and to reduce the number of mice used, in accordance with the European Communities Council Directive of 24 November 1986 (86/609/EEC). Transgenic mice: ATG5 floxable mice [80] were crossed with SLC17A6/Vglut2$^{ires\text{-}Cre/+}$ mice [81] and double mutant were used at 30 days (*atg5* cKO $n = 7$, *Atg5*$^{f/+}$ $n = 9$).

PT stroke was induced on anesthetized mice (isoflurane 1.2%) upon intraperitoneal injection of the photosensitive dye Rose Bengal (Sigma-Aldrich, 198,250; freshly prepared in sterile saline [10 mg/mL] and administered at the final dosage of 25 mg/kg). The dye was allowed to diffuse through the blood stream for 10 min. Mice were positioned on a stereotaxic frame (KOPF, 51,600 Lab Standard Stereotaxic Unit), the skull was exposed, and a fiber-optic bundle mounted on a cold light source (Coherent, OBIS 561 nm LS 120 mW laser system equipped with a fiber pigtail) set at 75 mW and kept at 1 mm far from the right skull surface (coordinates from bregma: AP: 0 mm; ML: 1.5 mm). Mice were illuminated for 5 min and during the surgical procedure, mice core body temperature was constantly monitored and kept at 37°C by a feedback heating pad (Rodent Warmer with Mouse Heating Pad 7 × 7 cm, RWD Life Science, 69,027). Next, the incision was sutured, and mice received the first compound intraperitoneal injection before returning to their housing cages. A group of mice received duloxetine treatment with a 4-h delay following stroke induction.

Drugs used *in vivo* were dissolved in DMSO at the final concentration of 15 mM. Animals were intraperitoneally injected with individual compound diluted in sterile saline or with vehicle (DMSO diluted in saline solution) in accordance with the experimental setting.

3-MA (Sigma-Aldrich, M9281) was dissolved in PEG 300/sterile saline 50% by heating and sonicating the solution to obtain 167 nmol/µL working solution; 3.6 µL of 3-MA was infused into the left cerebral ventricle (0.5 µL/min) at the following coordinates AP: 0 mm; ML: −0.5 mm; DV: −2.2 mm using an Infusion Syringe Pump (KDS Legato 130) coupled with the stereotaxic frame [17]. Mice then received Rose Bengal (i.p.) injection and 10 min after the delivery of photosensitive dye; the right hemisphere was exposed to light. Next, the incision was sutured, and mice returned in their cages.

The beam-walk test has been used as a reliable measure of locomotion. Mice were pre-treated the week before PT induction until they successfully walked across the 0.7 cm ×95 cm long beam without turning around and without any faults. Once the training is complete, mice are subjected to three consecutive testing trials to establish the baseline before operating the PT model. We measured the latency to traverse the beam, the average speed and the time they spent crawling the beam, Measurements were done 24 h and 48 h after the induction of the ischemic stroke. Data derives from the average of three runs.

MRI studies were performed on a 7T preclinical magnetic resonance scanner (Bruker, BioSpec 70/30 USR, Paravision 6.0.1, Germany), equipped with 450/675 mT/m gradients (slew-rate: 3400–4500T/m/s; rise-time: 140 µs). When performing *in vivo* MRI, animals were maintained under anesthesia with a mixture of isoflurane (1.2%) and O_2, and were placed in a bed with an integrated heating system to keep the body temperature at 37°C. A surface coil dedicated to mouse brain imaging was used to allow high signal quality and to acquire highly resolved images with the following sequences: Turbo spin-echo for T2-weighted images (TR = 3300 ms, TE = 50 ms, FOV = 16×16 mm, thickness = 0.650 mm) matrix size = 224x224, resolution = 0,071x0.071 mm). Volumetric analysis was done using the freeware MIPAV software.

To ensure unbiased procedures, all handling and experimental interventions, including treatment administration and outcome assessments, were conducted by personnel blinded to group assignments.

On the day of euthanasia, mice received an overdose of anesthetic drug, and they were perfused with saline solution containing 0.2% EDTA 0.5 M. For subsequent biochemical analyses (western blotting), brains were rapidly isolated, and coronal sections of stroked (right, ipsilateral) and contralateral (left) hemispheres were separately snap-frozen by immersion in liquid nitrogen and stored at −80°C before processing. The TTC labeling was obtained using coronal brain slices (2 mm) obtained by the vibratome Leica VT1200S. Sections were incubated in 1% 2,3,5-triphenyltetrazolium chloride (TTC; Sigma-Aldrich, T8877) staining solution (in PBS, filtered) for 30 min at 37°C, protected from light. Each slice was imaged on the posterior and anterior surfaces, and the TTC-unstained white area of the whole brain was measured as the infarct area.

For immunohistochemical analyses, brains were perfused with saline solution containing 0.2% EDTA 0.5 M, followed by 4% paraformaldehyde (PFA; Sigma-Aldrich, P6148) in PBS, pH 7.2. Next, brains were isolated and postfixed in 4% PFA/PBS solution for 12 h at 4°C. Tissues were cryoprotected with a 30% sucrose (Sigma-Aldrich, S7903)/PBS solution, embedded in OCT inclusion media (Bio-Optica, 05–9801), and stored at −80°C before processing. Brains were coronally sectioned (12 µm) and upon labeling sections were digitalized every 325 µm.

TEM was performed on brains perfused with saline solution containing 0.2% EDTA 0.5 M, followed by 2% PFA, 2.5% glutaraldehyde (Sigma-Aldrich, G5882) solution (prepared in sodium cacodylate). Brains were incubated in fixing solution for 12 h at 4°C, and subsequently sectioned.

Immunoblotting

For protein extraction, cells and tissues were washed with cold PBS and lysed in buffer containing the following: 50 mM Tris-HCl (Sigma-Aldrich, 93,362) pH 7.4, 150 mM NaCl (Sigma-Aldrich, S3014), 1% Triton X-100 (Sigma-Aldrich, 93,443), 0.5% sodium deoxycholate (Sigma-Aldrich, 30,968), 1 mM EDTA (Sigma-Aldrich, E6758), 10 mM NaF (Sigma-Aldrich, 201,154), 1 mM DTT (Sigma-Aldrich, 3860-OP), 1 mM EGTA (Sigma-Aldrich, 03777). For cell lysates, lysis buffer was supplemented with a 1X protease inhibitor cocktail (Sigma-Aldrich, P2714). For tissue samples, ipsilateral and contralateral cortices were homogenized in the above-described lysis buffer supplemented with 1X protease and phosphatase inhibitor cocktail (Sigma-Aldrich, PPC1010) using a glass pestle tissue grinder (on ice). Homogenates were then centrifuged at 13,500 x *g* for 10 min at 4°C (Eppendorf, Centrifuge 5424). Supernatants were collected and aliquoted in fresh tubes and stored at −80°C. Total protein concentration was measured with the bicinchronic acid (BCA) assay kit (Thermo Scientific, 23,225). Equal aliquots of protein (20–30 µg) were subjected to SDS-PAGE (7.5%, 10%, or 15% polyacrylamide gels), transferred to a nitrocellulose membrane using the Trans-Blot® Turbo™ Transfer System (Bio-Rad). Membranes were blocked with 5% nonfat dry milk or BSA (PBST 0.1%) and processed for incubation with primary and secondary HRP-conjugated antibodies (Bio-Rad, 1,706,515 and 1,706,516, 1:3000). The following primary antibodies were used in the present study: MAP1LC3B/LC3B (Novus Biologicals, NB100-200; 1:1000), SQSTM1/p62 (2C11; Novus Biologicals, H00008878-M01; 1:3000), HIF1A/HIF-1α (D2U3T; Cell Signaling Technology, 14,179; 1:1000), ACTB/β-actin (Sigma-Aldrich, A1978, 1:20000), ATG5 (D5F5U; Cell Signaling Technology, 12,994, 1:2000), BECN1 (Cell Signaling Technology, 3738, 1:2000), phospho-ULK1 (Ser757; Cell Signaling Technology, 6888, 1:1000), ULK1 (D8H5; Cell Signaling Technology, 8054, 1:1000), VCL/vinculin (clone V284; Merck, 05–386, 1:3000), phospho-RPS6KB/p70 S6 kinase (Thr389; Cell Signaling Technology, 9205; 1:1000), RPS6KB/p70 S6 kinase (Cell Signaling Technology, 9202, 1:1000), cleaved CASP3 (cCASP3, Asp175; Cell Signaling, 9664; 1:1000). After incubation, membranes were washed and reacted with enhanced chemiluminescence (ECL) reagent (Bio-Rad, 1,705,061). Images were acquired on Bio-Rad ChemiDoc Imager, and quantifications were done using the Image Lab 6.0.1 software (Bio-Rad).

Fluorescence microscopy and automatized immunohistochemistry (IHC)

Cells seeded on *ad hoc*-coated glass coverslips were washed with PBS, fixed with 2% PFA for 10 min, and incubated with 0.1 M glycine (Sigma-Aldrich, 50,046) for 10 min. For LC3 puncta imaging, PK-hLC3-expressing Neuro-2a cells were directly imaged by confocal microscopy using Leica TCS SP8 equipped with an HCX PL APO lambda blue 63.0x1.40 OIL UV objective or Olympus FluoVIEW 3000 RS equipped with UPLXAPO 60x1.42 OIL objective. Stacks (1024x1024) were post-processed to generate maximal projections of Z-stacks (acquired with a 0.3 µm step). Qualifications and imaging analyses were done using ImageJ (Fiji Version 2.0.0) and Leica Application Suite X software.

For IHC characterization of GFAP expression, brain cryosections were labeled with Automatic Leica BOND RX system (Leica Microsystems GmbH, Wetzlar, Germany). Sections were treated with the Epitope Retrieval Solution1 (ER1 Citrate Buffer) at 100°C before receiving the GFAP (Synaptic Systems, 173,002) rabbit antibody at the following dilution: 1:1000 (30 min, room temperature). The primary antibody was developed with Bond Polymer Refine Detection (Leica, DS9800). Slides were acquired with Aperio AT2 digital scanner at magnification of 40X (Leica Biosystems). Quantifications of $GFAP^+$ cells were done using QuPath 0.5.1. software. Standard IHC protocol for LC3B (rabbit; Invitrogen, 2H30L32, 1:1000) was used to detect LC3B on cortical sections [136].

Organoids were fixed in 4% PFA for 1 h at room temperature, washed 3 times in 1X PBS, and transferred to 30% w/v sucrose/PBS overnight at 4°C. They were then embedded in OCT, frozen in liquid nitrogen and isopentane, and stored at −80°C. For immunofluorescence analysis, 15-µm-thick sections were cut using a Leica cryostat. Cryosections were air-dried and rinsed twice with 1X PBS. Nonspecific binding sites were blocked by incubation with the blocking solution (1X

PBS, 0.1% Triton X-100, 10% donkey serum) for 1 h at room temperature. Cryosections were incubated with primary antibodies diluted in 1X PBS, 0.1% Triton X-100 (Sigma-Aldrich, X-100), and 1% donkey serum overnight at 4°C in a humidified chamber.

The following primary antibodies were used for immunofluorescence: GFAP (rabbit, DAKO, Z0334, 1:500); PLP1 (mouse, Invitrogen, MA1-80034, 1:100); MAP2 (mouse IgG1, clone AP20, Millipore, MAB3418, 1:250); GOLGA2/GM130 (mouse, BD bioscence, 610,822, 1:500); LAMP1 (mouse, Abcam, AB25630, 1:50); SQSTM1/p62 (rabbit, Sigma-Aldrich, P0067, 1:1000); TRPM2 (rabbit, Thermo Fisher, PA5-102844, 1:500), KDEL 10C3 (rabbit, ENZO, ADI-SPA-827-F, 1:400), CLDN5/claudin 5 (rabbit 34–1600, Invitrogen, 1:100). After incubation with the primary antibodies, cryosections were washed three times for 5 min with 1X PBS, 0.1% Triton X-100. Then, cryosections were incubated for 90 min at RT in the dark with appropriate donkey fluorophore-conjugated secondary antibodies (Alexa Fluor 555, Alexa Fluor 633, and Alexa Fluor 647), diluted in 1X PBS, 0.1% Triton X-100, 1% donkey serum. Nuclei were stained with DAPI (1:25,000; Roche) in 1X PBS for 3 min. IHC for CLDN5 was carried using biotin-secondary antibodies along with the Vector Elite ABC kit (PK6100) Sections were mounted with Dako fluorescent mounting medium and imaged on Olympus FluoVIEW 3000 RS confocal microscope under a 30X silicon objective. Images were processed in ImageJ (Fiji Version 2.0.0).

Transmission electron microscopy

In vitro TEM experiments involving naïve Neuro-2a were performed by plating cells in complete DMEM, at a density of 2.5×10^5 cells/well in 6-well multiple-well plates (Costar, 3516). Cells were allowed to grow for 24 h and subsequently cultured for 15 h in the presence of selected compounds at the final concentration of 10 µM, in combination with 100 nM Baf. TEM was performed on cells fixed in 2.5% glutaraldehyde (Sigma-Aldrich, G5882) solution for 1 h at room temperature. After fixation, cells were rinsed with 0.1 M sodium cacodylate (Sigma-Aldrich, C4945) buffer (pH 7.4). Cells were post-fixed in a solution containing: 1% OsO_4 (Sigma-Aldrich, 75,632), 1.5% $K_4Fe(CN)_6$ (Sigma-Aldrich, 702,587), and 0.1 M sodium cacodylate for 1 h at 4°C, protected from light. After fixation, cells were stained with 0.5% uranyl acetate at 4°C overnight, protected from light. Samples were next dehydrated using the following increasing concentration of ethanol: 30%, 50%, 70%, 80%, 90%, 96%, and 100%. After dehydration, samples were covered with a mixture of ethanol and epoxy resin (1:1), embedded in fresh epoxy resin (Sigma-Aldrich, 45,359), polymerized overnight at 45°C, and then incubated at 60°C for 24 h. Ultrathin sectioning (70 nm) was performed on a Leica EM UC6 ultramicrotome. Sections were positioned on 300-mesh square grids and contrasted with 2% aqueous uranyl acetate. *In vivo* TEM experiments were performed on brains perfused with saline solution containing 0.2% EDTA 0.5 M, followed by 2% PFA, 2.5% glutaraldehyde solution (prepared in sodium cacodylate). Brains were incubated in fixing solution for 12 h at 4°C, and subsequently post-fixed and sectioned as above. Images were collected using a FEI Tecnai-12 transmission electron microscope.

Neuro-vascular Unit construction and trans-endothelial cell electrical resistance monitoring

2×10^5 cm^{-2} primary brain glial cells were seeded on the abluminal side of matrix-coated Transwell™ tissue culture inserts (6.5-mm diameter, 3-µm pore size; Corning, 3415) and cultured for at least 2 h at 37°C. Transwell™ inserts were then flipped, and 25,000 cells/cm^2 primary brain endothelial cells were seeded on the lumenal side of matrix-coated inserts and co-cultured at 37°C for 7 days. Cells culture medium was changed every 2–3 days. For drugs analysis, 7B11 cells (1×10^5/well) were added baso-laterally to the NVU model, to mimic the neuronal component, and stimulated with DMSO (Ctrl) or Baf for 15 h, while the test compounds (duloxetine, NU7441, ONC212, and poziotinib) were added apically, to mimic a systemic treatment, in the presence (BBB plate) or absence (Ctrl plate) of the barrier prototype. *In vitro* barrier integrity was assessed by measuring TEER or by assessing the diffusion of fluorescent dextran (of various molecular weights). At least three independent preparations were analyzed, each with 4 replicates/conditions. The test compounds were administered on the apical side. TEER was assessed using a Voltohmeter (Millicell Electrical Resistance System, Millipore), and measurements were performed using the same settings to allow comparison of different conditions. Background resistance from cell-free matrix-coated transwells was subtracted from recorded values to determine absolute TEER which was then corrected for culturing area (in Ω^*cm^2). All measurements were repeated at least 3 times.

Dextran permeability assay

Solute paracellular permeability was assessed using 10 µg mL^{-1} 10 kDa-Dextran (Alexa Fluor® 555-conjugated, 10,000 MW; Molecular Probes, D22910) and 100 µg mL^{-1} 3 kDa-Dextran (Alexa Fluor® 488-conjugated, 3000 MW; Molecular Probes, D34682) in endothelial/glial Transwell™ co-cultures treated or untreated. NVU co-cultures were washed in PBS and pre-incubated for 5 min in FluoroBrite™ DMEM (Gibco, A1896701) medium at 37°C. Paracellular flux measurement was started by adding Dextran mixture to the upper chamber of the Transwell system, corresponding to the donor compartment. The basolateral (glial) side of the transwells represented the receiver side and was exposed to medium alone. Samples were incubated for 60 min at 37°C with slow continuous mixing. Samples were collected from the upper and lower chambers to quantify leakage of the fluorescent dye across the NVU prototype (apical to basolateral). The level of fluorescence in the collected media was measured for 488-Dextran ($\lambda ex = 495$ nm and $\lambda em = 519$ nm) or 555-Dextran ($\lambda ex = 555$ nm and $\lambda em = 565$ nm) by Synergy™ H4 Hybrid Multi-Mode Microplate Reader (BioTek). Relative fluorescence units were corrected for background fluorescence and converted to concentration according to standards. The amount of fluorescent test compound was calculated as

permeability coefficient (P_e, cm min^{-1}) and expressed as fold change of control cells [43].

Statistical analysis

Statistical analyses were performed using GraphPad Prism 9 software (GraphPad Software, LLC). Results are expressed as the mean value ± the standard deviation of the mean (SD). Normality was assessed using D'Agostino-Pearson normality test or Kolmogorov-Smirnov normality test. Comparisons were made using the following statistical tests: unpaired Student's *t*-test, one-way or two-way Analysis of Variance (ANOVA), followed by Tukey's or Šídák's multiple comparison tests, Chi-Square test; *p* values lower than 0.05 were considered statistically significant.

Power analysis was conducted using outcome variability observed in the first experimental cohort of mice (Figure 7C). The minimum sample size required for adequate statistical power (80%) at a significance level of $\alpha = 0.05$ was calculated using G*Power 3.1.9.6 and effect size estimation (2.05). The minimal sample size per group was determined to be 5 mice; therefore, all experiments were conducted with no fewer than five animals per group. Mathematical formulae of statistical measures used for the screening assay development and validation are herein reported. Values include means (μ), and standard deviations (σ). Colocalizations and analysis of immunofluorescence images were run on Fiji.

$$Z' - factor = 1 - \frac{3\left(\sigma_{samples} + \sigma_{controls}\right)}{\left|\mu_{samples} - \mu_{controls}\right|}$$

$$SSMD = \frac{\mu_{samples} - \mu_{controls}}{\sqrt{{\sigma_{samples}}^2 + {\sigma_{controls}}^2}}$$

$$S/N = \frac{\mu\left(C_{pos}\right) - \mu\left(C_{neg}\right)}{\sqrt{\sigma\left(C_{pos}\right)^2 + \sigma\left(C_{neg}\right)^2}}$$

$$Robust\ Z - score = \frac{S_i - median(S_{all})}{MAD(S_{all})}$$

$$MAD(S_{all}) = 1.4826 \times median(|S_i - median(S_{all})|)$$

Author contributions

CRediT: **Alice Viotti:** Conceptualization, Investigation, Methodology; **Claudia Molinaro:** Data curation, Investigation; **Jessica Perego:** Data curation, Investigation; **Andrea Fossaghi:** Investigation, Methodology; **Chiara Parravicini:** Data curation; **Eliana Lauranzano:** Investigation; **Antonella Borreca:** Investigation, Methodology; **Marco Piccoli:** Data curation, Investigation; **Luigi Anastasia:** Data curation; **Susanna Manenti:** Data curation; **Annamaria Finardi:** Data curation, Formal analysis; **Alessandra Mandelli:** Data curation, Formal analysis; **Michela Matteoli:** Conceptualization; **Ivano Eberini:** Investigation, Methodology; **Paola Panina:** Supervision; **Gianvito Martino:** Supervision; **Luca Muzio:** Conceptualization, Data curation, Formal analysis, Investigation, Methodology, Project administration.

Acknowledgements

We thank Dr. Rebecca Casula, Dr. Francesca Carriero, Dr. Margherita Ravanelli, and Dr. Valeria Mariotti, for their technical support. Figure 1A and S5E were created using pictures from Servier Medical Art, by Servier (http://smart.servier.com). The project was supported by Ministero della Salute Italiano with the following grant: RF-2016-02361571. This study is in memory of Giancarlo Comi, a great neurologist, the founder of the Institute of Experimental Neurology and a member of our scientific community.

Disclosure statement

No potential conflict of interest was reported by the author(s).

Funding

The work was supported by the Ministero della Salute [RF-2016-02361571].

Data availability statement

Original data in our study are available upon request

ORCID

Luca Muzio http://orcid.org/0000-0002-1068-865X

References

[1] Gbdsrf C, Abate MD, Abate YH. Global, regional, and national burden of stroke and its risk factors, 1990–2021: a systematic analysis for the Global Burden of Disease Study 2021. Lancet Neurol. 2024 Oct;23(10):973–1003. doi: 10.1016/S1474-4422(24)00369-7

[2] Powers WJ, Rabinstein AA, Ackerson T, et al. Guidelines for the early management of patients with acute ischemic stroke: 2019 update to the 2018 guidelines for the early management of acute ischemic stroke: a guideline for healthcare professionals from the American Heart Association/American Stroke Association. Stroke. 2019 Dec;50(12):e344–e418. doi: 10.1161/STR.0000000000000211

[3] Liu Y, Xue X, Zhang H, et al. Neuronal-targeted TFEB rescues dysfunction of the autophagy-lysosomal pathway and alleviates ischemic injury in permanent cerebral ischemia. Autophagy. 2019 Mar;15(3):493–509. doi: 10.1080/15548627.2018.1531196

[4] Egan DF, Shackelford DB, Mihaylova MM, et al. Phosphorylation of ULK1 (hATG1) by AMP-activated protein kinase connects energy sensing to mitophagy. Science. 2011 Jan 28;331(6016):456–461. doi: 10.1126/science.1196371

[5] Tan HWS, Sim AYL, Long YC. Glutamine metabolism regulates autophagy-dependent mTORC1 reactivation during amino acid starvation. Nat Commun. 2017 Aug 24;8(1):338. doi: 10.1038/s41467-017-00369-y

[6] Hwang JY, Gertner M, Pontarelli F, et al. Global ischemia induces lysosomal-mediated degradation of mTOR and activation of autophagy in hippocampal neurons destined to die. Cell Death Differ. 2017 Feb;24(2):317–329. doi: 10.1038/cdd.2016.140

[7] Guo K, Searfoss G, Krolikowski D, et al. Hypoxia induces the expression of the pro-apoptotic gene BNIP3. Cell Death Differ. 2001 Apr;8(4):367–376. doi: 10.1038/sj.cdd.4400810

[8] Rami A, Langhagen A, Steiger S. Focal cerebral ischemia induces upregulation of beclin 1 and autophagy-like cell death. Neurobiol Dis. 2008 Jan;29(1):132–141. doi: 10.1016/j.nbd.2007.08.005

[9] Koike M, Shibata M, Tadakoshi M, et al. Inhibition of autophagy prevents hippocampal pyramidal neuron death after hypoxic-ischemic injury. Am J Pathol. 2008 Feb;172(2):454–469. doi: 10.2353/ajpath.2008.070876

[10] Adhami F, Liao G, Morozov YM, et al. Cerebral ischemia-hypoxia induces intravascular coagulation and autophagy. Am J Pathol. 2006 Aug;169(2):566–583. doi: 10.2353/ajpath.2006.051066

[11] Qin AP, Liu CF, Qin YY, et al. Autophagy was activated in injured astrocytes and mildly decreased cell survival following glucose and oxygen deprivation and focal cerebral ischemia. Autophagy. 2010 Aug;6(6):738–753. doi: 10.4161/auto.6.6.12573

[12] Grishchuk Y, Ginet V, Truttmann AC, et al. Beclin 1-independent autophagy contributes to apoptosis in cortical neurons. Autophagy. 2011 Oct;7(10):1115–1131. doi: 10.4161/auto.7.10.16608

[13] Li WL, Yu SP, Chen D, et al. The regulatory role of NF-kappaB in autophagy-like cell death after focal cerebral ischemia in mice. Neuroscience. 2013 Aug 6;244:16–30. doi: 10.1016/j.neuroscience.2013.03.045

[14] Buckley KM, Hess DL, Sazonova IY, et al. Rapamycin up-regulation of autophagy reduces infarct size and improves outcomes in both permanent MCAL, and embolic MCAO, murine models of stroke. Exp Transl Stroke Med. 2014;6(1):8. doi: 10.1186/2040-7378-6-8

[15] Wei H, Li Y, Han S, et al. cPKCgamma-modulated autophagy in neurons alleviates ischemic injury in brain of mice with ischemic stroke through akt-mTOR pathway. Transl Stroke Res. 2016 Dec;7(6):497–511.

[16] Shi R, Weng J, Zhao L, et al. Excessive autophagy contributes to neuron death in cerebral ischemia. CNS Neurosci Ther. 2012 Mar;18(3):250–260. doi: 10.1111/j.1755-5949.2012.00295.x

[17] Wen YD, Sheng R, Zhang LS, et al. Neuronal injury in rat model of permanent focal cerebral ischemia is associated with activation of autophagic and lysosomal pathways. Autophagy. 2008 Aug;4(6):762–769. doi: 10.4161/auto.6412

[18] Forte M, Marchitti S, Cotugno M, et al. Trehalose, a natural disaccharide, reduces stroke occurrence in the stroke-prone spontaneously hypertensive rat. Pharmacol Res. 2021 Nov;173:105875. doi: 10.1016/j.phrs.2021.105875

[19] Yang Y, Chen S, Zhang Y, et al. Induction of autophagy by spermidine is neuroprotective via inhibition of caspase 3-mediated beclin 1 cleavage. Cell Death Dis. 2017 Apr 6;8(4):e2738. doi: 10.1038/cddis.2017.161

[20] Zhang X, Deguchi S, Deguchi K, et al. Amlodipine and atorvastatin exert protective and additive effects via antiapoptotic and antiautophagic mechanisms after transient middle cerebral artery occlusion in Zucker metabolic syndrome rats. J Neurosci Res. 2011 Aug;89(8):1228–1234. doi: 10.1002/jnr.22633

[21] Gao K, Wang G, Wang Y, et al. Neuroprotective effect of simvastatin via inducing the autophagy on spinal cord injury in the rat model. Biomed Res Int. 2015;2015:1–9. doi: 10.1155/2015/260161

[22] Hongyun H, Tao G, Pengyue Z, et al. Puerarin provides a neuroprotection against transient cerebral ischemia by attenuating autophagy at the ischemic penumbra in neurons but not in astrocytes. Neurosci Lett. 2017 Mar 16;643:45–51. doi: 10.1016/j.neulet.2017.02.009

[23] Yang Y, Gao K, Hu Z, et al. Autophagy upregulation and apoptosis downregulation in DAHP and triptolide treated cerebral ischemia. Mediators Inflamm. 2015;2015(1):120198. doi: 10.1155/2015/120198

[24] Tanida I, Ueno T, Uchiyama Y. A super-ecliptic, pHluorin-mKate2, tandem fluorescent protein-tagged human LC3 for the monitoring of mammalian autophagy. PLOS ONE. 2014;9(10):e110600. doi: 10.1371/journal.pone.0110600

[25] Yamamoto A, Tagawa Y, Yoshimori T, et al. Bafilomycin A1 prevents maturation of autophagic vacuoles by inhibiting fusion between autophagosomes and lysosomes in rat hepatoma cell line, H-4-II-E cells. Cell Struct Funct. 1998 Feb;23(1):33–42. doi: 10.1247/csf.23.33

[26] Thoreen CC, Kang SA, Chang JW, et al. An ATP-competitive mammalian target of rapamycin inhibitor reveals rapamycin-resistant functions of mTORC1. J Biol Chem. 2009 Mar 20;284(12):8023–8032. doi: 10.1074/jbc.M900301200

[27] Klionsky DJ, Elazar Z, Seglen PO, et al. Does bafilomycin A1 block the fusion of autophagosomes with lysosomes? Autophagy. 2008 Oct;4(7):849–850. doi: 10.4161/auto.6845

[28] Shvets E, Fass E, Elazar Z. Utilizing flow cytometry to monitor autophagy in living mammalian cells. Autophagy. 2008 Jul;4(5):621–628. doi: 10.4161/auto.5939

[29] Zhang XD, Kuan PF, Ferrer M, et al. Hit selection with false discovery rate control in genome-scale RNAi screens. Nucleic Acids Res. 2008 Aug;36(14):4667–4679. doi: 10.1093/nar/gkn435

[30] Gabryel B, Kost A, Kasprowska D. Neuronal autophagy in cerebral ischemia–a potential target for neuroprotective strategies? Pharmacol Rep. 2012;64(1):1–15. doi: 10.1016/S1734-1140(12)70725-9

[31] Tasca CI, Dal-Cim T, Cimarosti H. In vitro oxygen-glucose deprivation to study ischemic cell death. Methods Mol Biol. 2015;1254:197–210.

[32] Gabryel B, Kost A, Kasprowska D, et al. AMP-activated protein kinase is involved in induction of protective autophagy in astrocytes exposed to oxygen-glucose deprivation. Cell Biol Int. 2014 Oct;38(10):1086–1097. doi: 10.1002/cbin.10299

[33] Chen R, Lai UH, Zhu L, et al. Reactive oxygen species formation in the brain at different oxygen levels: the role of hypoxia inducible factors. Front Cell Dev Biol. 2018;6:132. doi: 10.3389/fcell.2018.00132

[34] Martin KR, Celano SL, Solitro AR, et al. A potent and selective ULK1 inhibitor suppresses autophagy and sensitizes cancer cells to nutrient stress. iScience. 2018 Oct 26;8:74–84. doi: 10.1016/j.isci.2018.09.012

[35] Golden EB, Cho HY, Hofman FM, et al. Quinoline-based antimalarial drugs: a novel class of autophagy inhibitors. Neurosurg Focus. 2015 Mar;38(3):E12. doi: 10.3171/2014.12.FOCUS14748

[36] Yoshii SR, Mizushima N. Monitoring and measuring autophagy. Int J Mol Sci. 2017 Aug 28;18(9):1865. doi: 10.3390/ijms18091865

[37] Kabeya Y, Mizushima N, Ueno T, et al. LC3, a mammalian homologue of yeast Apg8p, is localized in autophagosome membranes after processing. EMBO J. 2000 Nov 1;19(21):5720–5728.

[38] Poole B, Ohkuma S. Effect of weak bases on the intralysosomal pH in mouse peritoneal macrophages. J Cell Biol. 1981 Sep;90(3):665–669. doi: 10.1083/jcb.90.3.665

[39] Seglen PO, Gordon PB. 3-methyladenine: specific inhibitor of autophagic/lysosomal protein degradation in isolated rat hepatocytes. Proc Natl Acad Sci U S A. 1982 Mar;79(6):1889–1892. doi: 10.1073/pnas.79.6.1889

[40] Klionsky DJ, Abdel-Aziz AK, Abdelfatah S, et al. Guidelines for the use and interpretation of assays for monitoring autophagy 4th edition (1). Autophagy. 2021 Jan;17(1):1–382. doi: 10.1080/15548627.2020.1797280

[41] Tian J, Cheng J, Zhang J, et al. Protection of pyruvate against glutamate excitotoxicity is mediated by regulating DAPK1 protein complex. PLOS ONE. 2014;9(4):e95777. doi: 10.1371/journal.pone.0095777

[42] Petiot A, Ogier-Denis E, Blommaart EF, et al. Distinct classes of phosphatidylinositol 3'-kinases are involved in signaling pathways that control macroautophagy in HT-29 cells. J Biol Chem. 2000 Jan 14;275(2):992–998.

[43] Lauranzano E, Campo E, Rasile M, et al. A microfluidic human model of blood-brain barrier employing primary human astrocytes. Adv Biosyst. 2019 Jul;3(7):e1800335.

[44] de Ceglia R, Chaabane L, Biffi E, et al. Down-sizing of neuronal network activity and density of presynaptic terminals by pathological acidosis are efficiently prevented by Diminazene Aceturate. Brain Behav Immun. 2015 Mar;45:263–276. doi: 10.1016/j.bbi.2014.12.003

[45] Young JE, Martinez RA, La Spada AR. Nutrient deprivation induces neuronal autophagy and implicates reduced insulin signaling in neuroprotective autophagy activation. J Biol Chem. 2009 Jan 23;284(4):2363–2373. doi: 10.1074/jbc.M806088200

[46] Kline CL, Van den Heuvel AP, Allen JE, et al. ONC201 kills solid tumor cells by triggering an integrated stress response dependent on ATF4 activation by specific eIF2alpha kinases. Sci Signal. 2016 Feb 16;9(415):ra18.

[47] Komatsu M, Waguri S, Koike M, et al. Homeostatic levels of p62 control cytoplasmic inclusion body formation in autophagy-deficient

mice. Cell. 2007 Dec 14;131(6):1149–1163. doi: 10.1016/j.cell.2007.10.035
[48] Pankiv S, Clausen TH, Lamark T, et al. P62/SQSTM1 binds directly to Atg8/LC3 to facilitate degradation of ubiquitinated protein aggregates by autophagy. J Biol Chem. 2007 Aug 17;282(33):24131–24145. doi: 10.1074/jbc.M702824200
[49] Komatsu M, Kageyama S, Ichimura Y. P62/SQSTM1/A170: physiology and pathology. Pharmacol Res. 2012 Dec;66(6):457–462. doi: 10.1016/j.phrs.2012.07.004
[50] Chakrabarti L, Eng J, Ivanov N, et al. Autophagy activation and enhanced mitophagy characterize the Purkinje cells of PCD mice prior to neuronal death. Mol Brain. 2009 Jul 29;2:24. doi: 10.1186/1756-6606-2-24
[51] Kim KA, Kim D, Kim JH, et al. Autophagy-mediated occludin degradation contributes to blood-brain barrier disruption during ischemia in bEnd.3 brain endothelial cells and rat ischemic stroke models. Fluids Barriers CNS. 2020 Mar 14;17(1):21. doi: 10.1186/s12987-020-00182-8
[52] Lemieux B, Percival MD, Falgueyret JP. Quantitation of the lysosomotropic character of cationic amphiphilic drugs using the fluorescent basic amine red DND-99. Anal Biochem. 2004 Apr 15;327(2):247–251. doi: 10.1016/j.ab.2004.01.010
[53] Lee TK, Park JH, Ahn JH, et al. Pretreated duloxetine protects hippocampal CA1 pyramidal neurons from ischemia-reperfusion injury through decreases of glial activation and oxidative stress. J Neurol Sci. 2016 Nov 15;370:229–236. doi: 10.1016/j.jns.2016.09.059
[54] Demirdas A, Naziroglu M, Ovey IS. Duloxetine reduces oxidative stress, apoptosis, and Ca(2+) entry through modulation of TRPM2 and TRPV1 channels in the hippocampus and dorsal root ganglion of rats. Mol Neurobiol. 2017 Aug;54(6):4683–4695.
[55] Lange I, Yamamoto S, Partida-Sanchez S, et al. TRPM2 functions as a lysosomal Ca2± release channel in beta cells. Sci Signal. 2009 May 19;2(71):ra23.
[56] Kraft R, Grimm C, Frenzel H, et al. Inhibition of TRPM2 cation channels by N-(p-amylcinnamoyl)anthranilic acid. Br J Pharmacol. 2006 Jun;148(3):264–273. doi: 10.1038/sj.bjp.0706739
[57] Chen GL, Zeng B, Eastmond S, et al. Pharmacological comparison of novel synthetic fenamate analogues with econazole and 2-apb on the inhibition of TRPM2 channels. Br J Pharmacol. 2012 Nov;167(6):1232–1243. doi: 10.1111/j.1476-5381.2012.02058.x
[58] Watson BD, Dietrich WD, Busto R, et al. Induction of reproducible brain infarction by photochemically initiated thrombosis. Ann Neurol. 1985 May;17(5):497–504. doi: 10.1002/ana.410170513
[59] Labat-Gest V, Tomasi S. Photothrombotic ischemia: a minimally invasive and reproducible photochemical cortical lesion model for mouse stroke studies. J Vis Exp. 2013 Jun;9(76). doi: 10.3791/50370-v
[60] Yorimitsu T, Klionsky DJ. Autophagy: molecular machinery for self-eating. Cell Death Differ. 2005 Nov;12 Suppl 2(Suppl 2):1542–1552.
[61] Bederson JB, Pitts LH, Germano SM, et al. Evaluation of 2,3,5-triphenyltetrazolium chloride as a stain for detection and quantification of experimental cerebral infarction in rats. Stroke. 1986 Nov-Dec;17(6):1304–1308. doi: 10.1161/01.STR.17.6.1304
[62] Nitatori T, Sato N, Waguri S, et al. Delayed neuronal death in the CA1 pyramidal cell layer of the gerbil hippocampus following transient ischemia is apoptosis. J Neurosci. 1995 Feb;15(2):1001–1011. doi: 10.1523/JNEUROSCI.15-02-01001.1995
[63] Huang L, Liu Z, Wang L. Effects of ischemic post-conditioning on the expressions of LC3-II and Beclin-1 in the hippocampus of rats after cerebral ischemia and reperfusion. Open Life Sci. 2019 Jan;14(1):179–190. doi: 10.1515/biol-2019-0020
[64] Puyal J, Vaslin A, Mottier V, et al. Postischemic treatment of neonatal cerebral ischemia should target autophagy. Ann Neurol. 2009 Sep;66(3):378–389. doi: 10.1002/ana.21714
[65] Wei K, Wang P, Miao CY. A double-edged sword with therapeutic potential: an updated role of autophagy in ischemic cerebral injury. CNS Neurosci Ther. 2012 Nov;18(11):879–886. doi: 10.1111/cns.12005
[66] Leahy JJ, Golding BT, Griffin RJ, et al. Identification of a highly potent and selective DNA-dependent protein kinase (DNA-PK) inhibitor (NU7441) by screening of chromenone libraries. Bioorg Med Chem Lett. 2004 Dec 20;14(24):6083–6087. doi: 10.1016/j.bmcl.2004.09.060
[67] Lee SH, Kim CH. DNA-dependent protein kinase complex: a multifunctional protein in DNA repair and damage checkpoint. Mol Cells. 2002 Apr 30;13(2):159–166. doi: 10.1016/S1016-8478(23)15019-9
[68] Puustinen P, Keldsbo A, Corcelle-Termeau E, et al. Dna-dependent protein kinase regulates lysosomal amp-dependent protein kinase activation and autophagy. Autophagy. 2020 Oct;16(10):1871–1888. doi: 10.1080/15548627.2019.1710430
[69] Bryan MR, Uhouse MA, Nordham KD, et al. Phosphatidylinositol 3 kinase (PI3K) modulates manganese homeostasis and manganese-induced cell signaling in a murine striatal cell line. Neurotoxicology. 2018 Jan;64:185–194. doi: 10.1016/j.neuro.2017.07.026
[70] Matsumoto Y. Development and evolution of DNA-dependent protein kinase inhibitors toward cancer therapy. Int J Mol Sci. 2022 Apr 12;23(8):4264. doi: 10.3390/ijms23084264
[71] Zhao Y, Thomas HD, Batey MA, et al. Preclinical evaluation of a potent novel DNA-dependent protein kinase inhibitor NU7441. Cancer Res. 2006 May 15;66(10):5354–5362. doi: 10.1158/0008-5472.CAN-05-4275
[72] Bymaster FP, Lee TC, Knadler MP, et al. The dual transporter inhibitor duloxetine: a review of its preclinical pharmacology, pharmacokinetic profile, and clinical results in depression. Curr Pharm Des. 2005;11(12):1475–1493. doi: 10.2174/1381612053764805
[73] Knadler MP, Lobo E, Chappell J, et al. Duloxetine: clinical pharmacokinetics and drug interactions. Clin Pharmacokinet. 2011 May;50(5):281–294. doi: 10.2165/11539240-000000000-00000
[74] Li H, Zhang N, Lin HY, et al. Histological, cellular and behavioral assessments of stroke outcomes after photothrombosis-induced ischemia in adult mice. BMC Neurosci. 2014 May 2;15:58. doi: 10.1186/1471-2202-15-58
[75] Toda T, Yamamoto S, Umehara N, et al. Protective effects of duloxetine against cerebral ischemia-reperfusion injury via transient receptor potential melastatin 2 inhibition. J Pharmacol Exp Ther. 2019 Feb;368(2):246–254. doi: 10.1124/jpet.118.253922
[76] Howard G, Goff DC. Population shifts and the future of stroke: forecasts of the future burden of stroke. Ann N Y Acad Sci. 2012 Sep;1268(1):14–20. doi: 10.1111/j.1749-6632.2012.06665.x
[77] Adhami F, Schloemer A, Kuan CY. The roles of autophagy in cerebral ischemia. Autophagy. 2007 Jan-Feb;3(1):42–44. doi: 10.4161/auto.3412
[78] Wang JY, Xia Q, Chu KT, et al. Severe global cerebral ischemia-induced programmed necrosis of hippocampal CA1 neurons in rat is prevented by 3-methyladenine: a widely used inhibitor of autophagy. J Neuropathol Exp Neurol. 2011 Apr;70(4):314–322. doi: 10.1097/NEN.0b013e31821352bd
[79] Vanlandewijck M, He L, Mae MA, et al. A molecular atlas of cell types and zonation in the brain vasculature. Nature. 2018 Feb 22;554(7693):475–480. doi: 10.1038/nature25739
[80] Hara T, Nakamura K, Matsui M, et al. Suppression of basal autophagy in neural cells causes neurodegenerative disease in mice. Nature. 2006 Jun 15;441(7095):885–889. doi: 10.1038/nature04724
[81] Vong L, Ye C, Yang Z, et al. Leptin action on GABAergic neurons prevents obesity and reduces inhibitory tone to POMC neurons. Neuron. 2011 Jul 14;71(1):142–154. doi: 10.1016/j.neuron.2011.05.028
[82] Mizushima N, Yamamoto A, Matsui M, et al. In vivo analysis of autophagy in response to nutrient starvation using transgenic

mice expressing a fluorescent autophagosome marker. Mol Biol Cell. 2004 Mar;15(3):1101–1111. doi: 10.1091/mbc.e03-09-0704
[83] Fagiani F, Pedrini E, Taverna S, et al. A glia-enriched stem cell 3D model of the human brain mimics the glial-immune neurodegenerative phenotypes of multiple sclerosis. Cell Rep Med. 2024 Aug 20;5(8):101680. doi: 10.1016/j.xcrm.2024.101680
[84] Xia HG, Zhang L, Chen G, et al. Control of basal autophagy by calpain1 mediated cleavage of ATG5. Autophagy. 2010 Jan;6 (1):61–66. doi: 10.4161/auto.6.1.10326
[85] Hacke W, Kaste M, Bluhmki E, et al. Thrombolysis with alteplase 3 to 4.5 hours after acute ischemic stroke. N Engl J Med. 2008 Sep 25;359(13):1317–1329. doi: 10.1056/NEJMoa0804656
[86] Gravanis I, Tsirka SE. Tissue-type plasminogen activator as a therapeutic target in stroke. Expert Opin Ther Targets. 2008 Feb;12(2):159–170. doi: 10.1517/14728222.12.2.159
[87] Group ISTc, Sandercock P, Wardlaw JM, et al. The benefits and harms of intravenous thrombolysis with recombinant tissue plasminogen activator within 6 h of acute ischaemic stroke (the third international stroke trial [IST-3]): a randomised controlled trial. Lancet. 2012 Jun 23;379(9834):2352–2363.
[88] Emberson J, Lees KR, Lyden P, et al. Effect of treatment delay, age, and stroke severity on the effects of intravenous thrombolysis with alteplase for acute ischaemic stroke: a meta-analysis of individual patient data from randomised trials. Lancet. 2014 Nov 29;384(9958):1929–1935. doi: 10.1016/S0140-6736(14)60584-5
[89] Mizushima N, Noda T, Yoshimori T, et al. A protein conjugation system essential for autophagy. Nature. 1998 Sep 24;395 (6700):395–398. doi: 10.1038/26506
[90] Denton D, Nicolson S, Kumar S. Cell death by autophagy: facts and apparent artefacts. Cell Death Differ. 2012 Jan;19(1):87–95. doi: 10.1038/cdd.2011.146
[91] Fan J, Zhang Z, Chao X, et al. Ischemic preconditioning enhances autophagy but suppresses autophagic cell death in rat spinal neurons following ischemia-reperfusion. Brain Res. 2014 May 8;1562:76–86. doi: 10.1016/j.brainres.2014.03.019
[92] Galluzzi L, Bravo-San Pedro JM, Blomgren K, et al. Autophagy in acute brain injury. Nat Rev Neurosci. 2016 Aug;17(8):467–484. doi: 10.1038/nrn.2016.51
[93] Wang P, Xu TY, Wei K, et al. ARRB1/beta-arrestin-1 mediates neuroprotection through coordination of BECN1-dependent autophagy in cerebral ischemia. Autophagy. 2014 Sep;10 (9):1535–1548. doi: 10.4161/auto.29203
[94] Papadakis M, Hadley G, Xilouri M, et al. Tsc1 (hamartin) confers neuroprotection against ischemia by inducing autophagy. Nat Med. 2013 Mar;19(3):351–357. doi: 10.1038/nm.3097
[95] Zeng XJ, Li P, Ning YL, et al. Impaired autophagic flux is associated with the severity of trauma and the role of A(2A)R in brain cells after traumatic brain injury. Cell Death Dis. 2018 Feb 14;9 (2):252. doi: 10.1038/s41419-018-0316-4
[96] Chauhan A, Sharma U, Jagannathan NR, et al. Rapamycin protects against middle cerebral artery occlusion induced focal cerebral ischemia in rats. Behav Brain Res. 2011 Dec 1;225 (2):603–609. doi: 10.1016/j.bbr.2011.08.035
[97] Sheng R, Zhang LS, Han R, et al. Autophagy activation is associated with neuroprotection in a rat model of focal cerebral ischemic preconditioning. Autophagy. 2010 May;6(4):482–494. doi: 10.4161/auto.6.4.11737
[98] Su J, Zhang T, Wang K, et al. Autophagy activation contributes to the neuroprotection of remote ischemic perconditioning against focal cerebral ischemia in rats. Neurochem Res. 2014 Nov;39 (11):2068–2077. doi: 10.1007/s11064-014-1396-x
[99] Zheng C, Han J, Xia W, et al. NAD(+) administration decreases ischemic brain damage partially by blocking autophagy in a mouse model of brain ischemia. Neurosci Lett. 2012 Mar 23;512(2):67–71.
[100] Lipinski CA, Lombardo F, Dominy BW, et al. Experimental and computational approaches to estimate solubility and permeability in drug discovery and development settings. Adv Drug Deliv Rev. 2001 Mar 1;46(1–3):3–26.
[101] De Rycker M, Baragana B, Duce SL, et al. Challenges and recent progress in drug discovery for tropical diseases. Nature. 2018 Jul;559(7715):498–506. doi: 10.1038/s41586-018-0327-4
[102] Agamah FE, Mazandu GK, Hassan R, et al. Computational/in silico methods in drug target and lead prediction. Brief Bioinform. 2020 Sep 25;21(5):1663–1675. doi: 10.1093/bib/bbz103
[103] Galindez G, Matschinske J, Rose TD, et al. Lessons from the COVID-19 pandemic for advancing computational drug repurposing strategies. Nat Comput Sci. 2021 Jan;1(1):33–41. doi: 10.1038/s43588-020-00007-6
[104] Tanida I, Tanida-Miyake E, Ueno T, et al. The human homolog of Saccharomyces cerevisiae Apg7p is a protein-activating enzyme for multiple substrates including human Apg12p, GATE-16, GABARAP, and MAP-LC3. J Biol Chem. 2001 Jan 19;276 (3):1701–1706. doi: 10.1074/jbc.C000752200
[105] Tanida I, Tanida-Miyake E, Komatsu M, et al. Human Apg3p/Aut1p homologue is an authentic E2 enzyme for multiple substrates, GATE-16, GABARAP, and MAP-LC3, and facilitates the conjugation of hApg12p to hApg5p. J Biol Chem. 2002 Apr 19;277 (16):13739–13744. doi: 10.1074/jbc.M200385200
[106] Goldberg MP, Choi DW. Combined oxygen and glucose deprivation in cortical cell culture: calcium-dependent and calcium-independent mechanisms of neuronal injury. J Neurosci. 1993 Aug;13 (8):3510–3524. doi: 10.1523/JNEUROSCI.13-08-03510.1993
[107] Goktug SCCaTc AN. Data analysis approaches in high throughput screening[book chapter]. Drug Discov. 2013 7:201–226.
[108] Chan PH. Reactive oxygen radicals in signaling and damage in the ischemic brain. J Cereb Blood Flow Metab. 2001 Jan;21(1):2–14. doi: 10.1097/00004647-200101000-00002
[109] Shackelford DA, Tobaru T, Zhang S, et al. Changes in expression of the DNA repair protein complex DNA-dependent protein kinase after ischemia and reperfusion. J Neurosci. 1999 Jun 15;19(12):4727–4738. doi: 10.1523/JNEUROSCI.19-12-04727.1999
[110] Woo RA, McLure KG, Lees-Miller SP, et al. DNA-dependent protein kinase acts upstream of p53 in response to DNA damage. Nature. 1998 Aug 13;394(6694):700–704. doi: 10.1038/29343
[111] Liu GY, Sabatini DM. mTOR at the nexus of nutrition, growth, ageing and disease. Nat Rev Mol Cell Biol. 2020 Apr;21 (4):183–203. doi: 10.1038/s41580-019-0199-y
[112] Cano C, Saravanan K, Bailey C, et al. 1-substituted (dibenzo[b,d] thiophen-4-yl)-2-morpholino-4H-chromen-4-ones endowed with dual DNA-PK/PI3-K inhibitory activity. J Med Chem. 2013 Aug 22;56(16):6386–6401. doi: 10.1021/jm400915j
[113] Rosenblum WI, El-Sabban F. Effects of combined parenchymal and vascular injury on platelet aggregation in pial arterioles of living mice: evidence for release of aggregate-inhibiting materials. Stroke. 1977 Nov-Dec;8(6):691–693. doi: 10.1161/01.STR.8.6.691
[114] Granger DN, Kvietys PR. Reperfusion injury and reactive oxygen species: the evolution of a concept. Redox Biol. 2015 Dec;6:524–551. doi: 10.1016/j.redox.2015.08.020
[115] Culmsee C, Bondada S, Mattson MP. Hippocampal neurons of mice deficient in DNA-dependent protein kinase exhibit increased vulnerability to DNA damage, oxidative stress and excitotoxicity. Brain Res Mol Brain Res. 2001 Mar 5;87(2):257–262. doi: 10.1016/S0169-328X(01)00008-0
[116] Wong DT, Robertson DW, Bymaster FP, et al. LY227942, an inhibitor of serotonin and norepinephrine uptake: biochemical pharmacology of a potential antidepressant drug. Life Sci. 1988;43(24):2049–2057. doi: 10.1016/0024-3205(88)90579-6
[117] Khan AY, Macaluso M. Duloxetine for the treatment of generalized anxiety disorder: a review. Neuropsychiatr Dis Treat. 2009;5:23–31.
[118] Mallinckrodt CH, Watkin JG, Liu C, et al. Duloxetine in the treatment of major depressive disorder: a comparison of efficacy in patients with and without melancholic features. BMC Psychiatry. 2005 Jan 4;5(1):1. doi: 10.1186/1471-244X-5-1
[119] Moore RA, Cai N, Skljarevski V, et al. Duloxetine use in chronic painful conditions–individual patient data responder analysis. Eur J Pain. 2014 Jan;18(1):67–75. doi: 10.1002/j.1532-2149.2013.00341.x

[120] Mahesh B, Singh VK, Pathak A, et al. Efficacy of duloxetine in patients with central post-stroke pain: a randomized double blind placebo controlled trial. Pain Med. 2023 Jun 1;24(6):610–617. doi: 10.1093/pm/pnac182
[121] Vranken JH, Hollmann MW, van der Vegt MH, et al. Duloxetine in patients with central neuropathic pain caused by spinal cord injury or stroke: a randomized, double-blind, placebo-controlled trial. Pain. 2011 Feb;152(2):267–273. doi: 10.1016/j.pain.2010.09.005
[122] Kim NY, Lee SC, Kim YW. Effect of duloxetine for the treatment of chronic central poststroke pain. Clin Neuropharmacol. 2019 May/Jun;42(3):73–76. doi: 10.1097/WNF.0000000000000330
[123] Wang Q, Guo W, Hao B, et al. Mechanistic study of TRPM2-Ca(2+)-CAMK2-BECN1 signaling in oxidative stress-induced autophagy inhibition. Autophagy. 2016 Aug 2;12(8):1340–1354. doi: 10.1080/15548627.2016.1187365
[124] Wang SY, Calderon J, Kuo Wang G. Block of neuronal Na+ channels by antidepressant duloxetine in a state-dependent manner. Anesthesiology. 2010 Sep;113(3):655–665. doi: 10.1097/ALN.0b013e3181e89a93
[125] Park JA, Lee CH. Neuroprotective effect of duloxetine on chronic cerebral hypoperfusion-induced hippocampal neuronal damage. Biomol Ther (Seoul). 2018 Mar 1;26(2):115–120. doi: 10.4062/biomolther.2016.248
[126] Alim I, Teves L, Li R, et al. Modulation of NMDAR subunit expression by TRPM2 channels regulates neuronal vulnerability to ischemic cell death. J Neurosci. 2013 Oct 30;33(44):17264–17277. doi: 10.1523/JNEUROSCI.1729-13.2013
[127] Gelderblom M, Melzer N, Schattling B, et al. Transient receptor potential melastatin subfamily member 2 cation channel regulates detrimental immune cell invasion in ischemic stroke. Stroke. 2014 Nov;45(11):3395–3402. doi: 10.1161/STROKEAHA.114.005836
[128] Lee M, Cho T, Jantaratnotai N, et al. Depletion of GSH in glial cells induces neurotoxicity: relevance to aging and degenerative neurological diseases. FASEB J. 2010 Jul;24(7):2533–2545. doi: 10.1096/fj.09-149997
[129] Hwang HY, Shim JS, Kim D, et al. Antidepressant drug sertraline modulates AMPK-MTOR signaling-mediated autophagy via targeting mitochondrial VDAC1 protein. Autophagy. 2021 Oct;17(10):2783–2799. doi: 10.1080/15548627.2020.1841953
[130] Cho YS, Yen CN, Shim JS, et al. Antidepressant indatraline induces autophagy and inhibits restenosis via suppression of mTOR/S6 kinase signaling pathway. Sci Rep. 2016 Oct 3;6:34655. doi: 10.1038/srep34655
[131] Yang Y, Hu Z, Du X, et al. MiR-16 and fluoxetine both reverse autophagic and apoptotic change in chronic unpredictable mild stress model rats. Front Neurosci. 2017;11:428. doi: 10.3389/fnins.2017.00428
[132] Reinhardt P, Glatza M, Hemmer K, et al. Derivation and expansion using only small molecules of human neural progenitors for neurodegenerative disease modeling. PLOS ONE. 2013;8(3):e59252. doi: 10.1371/journal.pone.0059252
[133] Rasile M, Lauranzano E, Faggiani E, et al. Maternal immune activation leads to defective brain-blood vessels and intracerebral hemorrhages in male offspring. EMBO J. 2022 Dec 1;41(23):e111192.
[134] Fossati G, Pozzi D, Canzi A, et al. Pentraxin 3 regulates synaptic function by inducing AMPA receptor clustering via ECM remodeling and beta1-integrin. EMBO J. 2019 Jan 3;38(1):e99529.
[135] Arenas A, Kuang L, Zhang J, et al. FUS regulates autophagy by mediating the transcription of genes critical to the autophagosome formation. J Neurochem. 2021 May;157(3):752–763. doi: 10.1111/jnc.15281
[136] Muzio L, Cavasinni F, Marinaro C, et al. Cxcl10 enhances blood cells migration in the sub-ventricular zone of mice affected by experimental autoimmune encephalomyelitis. Mol Cell Neurosci. 2010 Mar;43(3):268–280. doi: 10.1016/j.mcn.2009.11.008